LICENTIATE THESIS

Stiffness Characterization in Non-Crimp Fabric Composites

Hana Zrida Ammar

LULEÅ UNIVERSITY OF TECHNOLOGY

Stiffness characterization in Non-Crimp Fabric Composites

LICENTIATE THESIS

Hana Zrida Ammar

Division of Materials Science
Department of Engineering Sciences and Mathematics
Luleå University of Technology
Luleå, Sweden
SE 97187

February 2014

Printed by Luleå University of Technology, Graphic Production 2014

ISSN: 1402-1757
ISBN 978-91-7439-832-8 (print)
ISBN 978-91-7439-833-5 (pdf)

Luleå 2014

www.ltu.se

Preface

The work presented in this thesis contains two scientific papers that summarize my work performed within the Division of Materials Science in Luleå University of Technology in Sweden and in the Division of Mechanics of Materials (SI2M) in Jean Lamour Institute in France during the period from October 2011 to December 2013.

This thesis could not have seen the light of day without the precious support of many persons.

There is no way I can ever thank my mentor Professor Janis Varna for his unconditional and unswerving help, for his precious time, for his valuable advice, for his patience and for his willingness to listen and his whole-hearted readiness to help when I most need it. Words just fail me whenever I try to express my gratitude for him, and I wish I could coin a stronger expression that merely saying "Thank you!". Until then, I would say: "You give but little when you give of your possessions- It is when you give of yourself that you truly give", THANK YOU for making my research experience ever so unique.

I would like to express also my sincerest gratitude to my supervisor in France Professor Zoubir Ayadi for his support and guidance and for his fruitful suggestions and remarks.

I gratefully acknowledge my co-author Dr. Erik Marklund for his assistance in my research and for shearing his knowledge and for his contributions.

It is a pleasure to thank the Joint European Doctoral Program in Material Science and Engineering (DocMase) for financing this project.

I would like to offer my special thanks to Professor Zouhir Fakhfakh from my home country (Tunisia) for his encouragement and his personal support. Special thanks go also to Professor Roberts Joffe and Dr. Lennart Wallström for their kind help. Many thanks go to my colleagues and my friends who were important to the successful realization of my thesis.

Finally, I owe my deepest gratitude to my relatives, my parents, my brother and my husband for their love, prayer, support, care and encouraging words that light my way and kindle my enthusiasm to bring out the best in me in all my academic endeavors.

Luleå, February 2014

Hana Zrida Ammar

Abstract

Lightweight materials with high stiffness and damage tolerance are requested for aerospace, marine and automotive industries. Many types of composite materials are today used in various types of load carrying structures, due to their excellent strength and stiffness to weight ratio. Simplicity, reliability and low cost of the material processing are important factors affecting the final selection. In the last years new types of composites; Non-crimp-fabric (NCF) reinforced composites, where the cost-efficiency is reached by using dry preforms which are impregnated by resin infusion, resin transfer molding etc.; have made a break-through and have been widely used.

As its names indicates, NCF composites consist of layers with ideally straight fiber bundles oriented in different directions, knitted by secondary yarn and separated by resin. This technique of dry preforms impregnated by resin infusion or RTM combine a perfect placement of reinforcement with easy, cheap and automated manufacturing. It produces a composite that can be formed easily in complex shapes, with improvement in damage tolerance as well as the out-of-plane fracture toughness.

However, the stitching distorts and crimps the fiber bundles, which leads to large out-of-plane waviness. This deviation affects the mechanical properties of NCF composites. The bundle crimps reduces the stiffness and causes incorrect predictions of the laminate elastic properties employing assumption of the classical laminate theory (CLT).

In the present study, the fiber tow waviness is assumed as sinusoidal and the undulation effect on the stiffness reduction is analyzed using Finite Element Method (FEM). The waviness parameters i.e. wavelength and amplitude as well as geometrical parameters like bundle thickness are used in modeling the elastic properties of the representative volume element of the waved structure using meso-scale FEM analysis.

The possibility of applying CLT for cross-ply NCF composite stiffness determination is approved, by replacing the curved structure by idealized straight one using effective stiffness for the 0^o- and the 90^o- layers. The cross-ply NCF stiffness reduction is dominated by the stiffness reduction of the 0^o-layer. The 0^o-layer effective stiffness can be determined either by modeling a single curved tow subjected to distributed load, to reproduce its interaction with the neighboring layers, together with symmetry boundary conditions, or using a master curve approach, where a knock down factor is introduced to characterize the stiffness reduction and analytical expression is suggested. This expressions allows for determination of knock down factor for any given wavelength and amplitude of the waviness.

List of appended papers

Paper A

H. Zrida, E. Marklund, J. Varna and Z. Ayadi. Effective stiffness of 0^o-layer for stiffness determination of cross-ply non-crimp fabric composites. Journal of reinforced plastics and composites, submitted, 2014.

Paper B

H. Zrida, E. Marklund, J. Varna and Z. Ayadi. Master curve approach to axial stiffness calculation of biaxial composites with bundle waviness. Composites Part B: Engineering, submitted 2014.

Contents

1. Introduction

1.1. Fiber reinforced composites

The quest of weight gain using materials with superior specific properties, engages the interest of many researches to explore composite materials. Each year, composites find their way into hundreds of new applications from golf clubs and tennis rackets to jet skis, aircraft, missiles and spacecraft.

Composite materials are widely used in different areas such as aeronautics (helicopter blades, pressure bulkhead, cargo door, etc), maritime transport (boats, etc), automotive industry (car roof, car carline, etc), electronic (insulation, mounting printed circuit, boards, etc), buildings (furniture, roofing, etc), industry (tanks, pipes, wind turbine blades, etc) and even in sports and entertainment (skis, fishing rods, helmets, etc)…

A composite material consists of an assembly of different immiscible materials which complement each other and bring about a material whose physical properties are better than those of the individual constituents working separately.

Polymer composites are formed with reinforcement in the form of particles or fibers embedded in a matrix. The matrix is often a thermoplastic or a thermoset polymer. The matrix preserves the geometric arrangement of fibers, protects them from the environmental attack and damage, to which the sample can be exposed. The fibers can have inorganic or organic nature such as carbon fibers, glass fibers, oxide fibers, silicon carbide fibers, etc. They can be continuous or discontinuous filaments. The high stiffness and strength of polymer composite materials stems from the high stiffness and strength of fibers. Their geometry allows them to have minimal defects and their composition gives them a high strength. The fibers work as reinforcements since the load is transferred to them from the matrix. The volume fraction of fibers for a structural composite is typically 45%-65%. The maximum theoretical value is 79% for square array and 91% for a hexagonal array **[1]**.

The fibers can be arranged in different ways: homogenously or uniformly dispersed like in pre-impregnated tape laminates or in form of bundles like in the woven reinforced composites or the non-crimp fabric composites.

The pre-impregnated tape laminate, shown in **Figure1 [2]**, is a stack of unidirectional plies in which the layers are perfectly bonded to each other and the mechanical properties depend on their orientations.

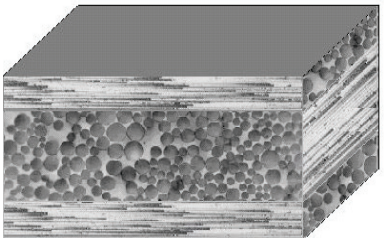

Figure1. Internal structure of pre impregnated tape based cross ply laminate **[2]**

The main advantage of this material is the high fiber volume fraction that can be obtained with well aligned fibers, showing an excellent in-plane stiffness and strength. The problem with this material is that it is expensive. The high costs combine the high labor costs and the high storing costs (pre-impregnated tapes require low temperature to prevent curing). Another drawback is the sensitivity to inter-layer delamination cracking under impact loading due to their poor interlaminar fracture toughness **[3]**.

This problem is solved with woven composites shown in **Figure2 [4]**, the reinforcing fibers are assembled in bundles in different directions and form a fabric.

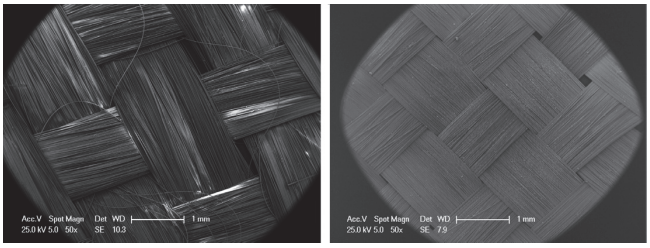

Figure2. Images of E-glass (left) and basalt (right) woven fabrics **[4]**

This composite has two-directional reinforcement and its manufacturing cost is lower than that of the pre-impregnated tape based composite. The woven structure shows high waviness in the out-of-plane direction. This waviness brings advantages to the material by improving its fracture toughness and its mechanical properties in the out-of-plane direction. But, it brings also significant drawbacks to woven composite by reducing the in-plane properties.

Some drawbacks of the pre-impregnated tape based composites and of the woven composites are overcome with new type of textile composite called non-crimp-fabric composites (NCF) presented in **Figure3 [5]**.

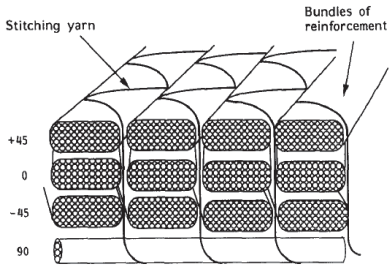

Figure5. Schematic diagram showing a multi-axial non-crimp fabric **[5]**

NCFs are relatively new class of textiles in which a fabric is constructed of layers of fiber bundles aligned in specific directions **[6]**. The layers of fibers are produced by laying tows next to each other in a specified direction and subsequently employing a secondary fine yarn knitted around the tows to hold the fabric in place. The use of through-thickness stitching allows for improvement in damage tolerance and in the interlaminar fracture toughness. The manufacturing technique provides a dry preform which can be used in complicated shapes before it is consolidated into the final composite by resin transfer molding with low manufacturing costs comparing to the pre-impregnated tape based composite. NCF composites, ideally, would combine a good in-plane response, like pre-impregnated tape based composites and the good through-thickness stiffness and strength due to the stitching in the thickness direction **[7]**.

NCFs show heterogeneities in the micro- and the meso –scale as shown in **Figure4 [8]**. The micro-scale heterogeneity can be seen from the microstructure of the fiber-matrix inside the bundles, the meso-scale heterogeneity is due to the structure of layers where the fiber bundles are separated by the matrix.

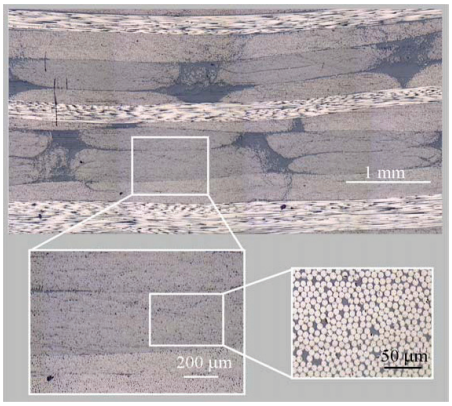

Figure4. Hierarchical structure of the NCF composites **[8]**

As it is shown in **Figure4**, the 0°-tows are far from being ideally oriented and present waviness in the out-of-plane direction. The stitching yarn induces waviness which leads to the in-plane stiffness reduction. The waviness occurring in NCF composites are similar to that can be seen in woven reinforced composites with lower amplitudes.

1.2. Modeling approaches

In order to study the mechanical properties dependence on the architecture parameters, finite element analysis and theoretical analysis methods are more convenient than the experimental techniques because of the complex geometry.

Finite element method (FE) started with Ritz who developed an effective method for an approximate solution of problems in the mechanics of deformable solids **[9-10]**. FE is a numerical method for finding approximate solutions to boundary value problems for differential equations. It uses variational methods to minimize an error function and produces a stable solution. The problem is transformed to an equivalent one in terms of properties and geometry and the method is based on the

discretization principle which is translated by the choice of a mesh that occurs by dividing the studied area into sub-domains with simple geometry (triangle, quadrilateral, etc) and with finite dimensions, hence the finite element method's name. Results are determined for each element. The accuracy of the results is directly related to the mesh quality realized (number of element, their distribution in the structure, form of element, etc). In FE analysis many errors can be produced, such as wrong interpretations of the physical model, mechanical modeling errors due to many assumptions like geometric simplifications and resolution errors which are due to problems of numerical accuracy. The engineer must be aware of the existence of these errors and must be able to estimate a level of confidence in the results.

Many researches have been conducted for predicting the mechanical properties of textile composites. The basic principle to determine the elastic properties of a textile composite using FE is to divide the structure into unit cells and then mechanical properties are calculated for the unit cell.

Since the textile composites have a complex architecture it is not easy to incorporate all geometrical parameters and simplifications needed in the FE modeling **[11]**.

Naik et al. **[12-14]** proposed a 2D crimp model for the elastic analysis of a 2D plain weave. The unit cell in this model was divided into sections and then the series-parallel models were used to estimate the lower and the upper bounds of the elastic constants.

Ishikawa and Chou developed the "mosaic" model **[15]**, the "fiber undulation" model **[16]** and further the "bridging" model **[17]** for analyzing the elastic behavior of woven hybrid composites. In these models a fabric composite was simply regarded as an assembly of blocks of cross-ply laminates neglecting the shear deformation in the thickness direction.

Byström at al. **[18]** developed a homogenization method for stiffness matrix computation of woven composites; the method was called reiterated

homogenization. The authors studied the linear elastic problems with periodic microstructure, which justifies the use of representative volume element which is enough to represent the elastic properties of the whole material.

More recent study was performed by Riccio et al. **[19]** who developed a representative volume element (RVE) for NCF composites under tension loading taking into account the tow's waviness and the stitching. The classical micromechanical theory was used together with the stiffness averaging method. It was demonstrated that the exclusion of the tow's waviness from the model leads to a big error of the stiffness comparing to the experimental data. However, the lack of stitching in the model is less relevant leading to a small error that can be neglected. The stiffness dependence on the tow's waviness was investigated and it was shown that this stiffness strongly depends on the waviness.

A mesoscopic FE model of the NCF structure was realized by Drapier **[20]** in order to investigate the interlaminar shear behavior of non-crimp fabric composites. The geometrical heterogeneity was taken into account. The tow's crimp was considered large enough for the composite to be regarded between the pre-impregnated tapes and the woven structures. This waviness was assumed as sinusoidal shaped characterized by a wavelength and amplitude. The same assumption was used in **[21]** by Edgren et al. where the authors used Timoshenko beam theory in addition to FE to calculate the stiffness of a layer in the NCF composite considered like a single curved beam. In addition to this assumption, Mattsson et al. **[22]** demonstrated that the 90°-layer with bundle mesostructure can be replaced by homogenized 90°-layer without losing accuracy in the NCF laminate stiffness investigation.

2. Summary of appended papers

The assumptions mentioned in the previous paragraph helped for the NCF modeling in the present study. The objective of the work is to realize a model for the NCF composite mesostructure in the attempt to investigate the effect of the waviness on the stiffness reduction. Moreover, the stiffness calculation methods of for the

complex geometry are explained and justified and finally, the different geometrical parameters changes are taken into consideration and included in the calculation.

For this purpose, the modeling is performed through different length scales (See **Fig.5**). Starting with the micro scale modeling, the fiber with transversely isotropic properties is embedded in the matrix with isotropic properties forming a micromechanics model for a unidirectional composite. This model has certain fibers content and fibers are assumed hexagonally packed **[23]**.

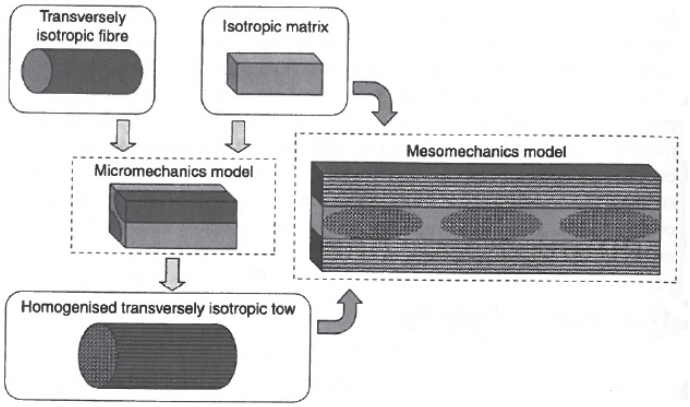

Figure5. Modeling stiffness properties for non-crimp fabric composites using multi-scale analysis **[23]**

The elastic properties of the unidirectional composite are used as input in the second level of modeling. The 0^{o}-tows and the 90^{o}-bundles are considered as homogenized transversely isotropic material. The meso scale modeling of cross ply NCF composite is realized by following a sinus shaped functions for the geometry and by modeling a representative unit cell (RUC) that can represent a part of the structure after applying symmetry conditions (see **Figure6**).

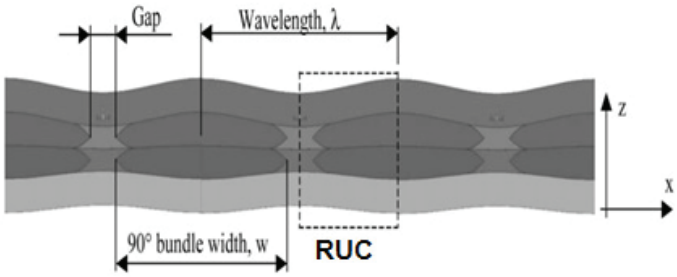

Figure6. A cross ply NCF composite with mid-plane symmetry, the representative unit cell is marked by dashed line **[24]**

The stiffness of NCF composite is calculated using FE method. It is shown that it strongly depends on the geometrical parameters: the waviness's amplitude and wavelength. The classical laminate theory cannot be directly applied to a curved cross ply NCF structures to calculate their axial stiffness, contrarily to the flat laminate where classical laminate theory can be reduced to a simple rule of mixture combining the longitudinal and the transverse stiffness of each layer. It is demonstrated in this thesis that classical laminate theory can be applied to calculate the NCF composite stiffness by replacing the curved structure with idealized straight one using what we called "effective stiffness" for each layer, the problem remains the determination of the effective stiffness for all amplitudes and wavelengths.

Two approaches are developed in this work and are presented in two separate papers:

In **paper A**, a single curved 0^{o}-tow is modeled and is subjected to periodic distributed load as boundary conditions together with symmetry conditions in order to reproduce its interaction with the neighboring layers (in our case the 90^{o}-layer). The local stress distribution at the interface between the layers in NCF composite is investigated. It is shown that the normal and shear stresses are changing according a sinus shaped functions. The same kind of function used in the geometry modeling is used to fit the stresses as a function of the coordinate. The fitting expressions can be used when applying boundary conditions in analytical models to calculate the

effective stiffness of the 0^{o}-tow. The distributed load is deduced from the stresses expressions and considered as adequate boundary conditions which lead to an accurate calculation of the effective stiffness of the curved 0^{o}-tow that can be used in classical laminate theory to find the NCF composite stiffness for any given amplitude and wavelength of the waviness.

In **Paper B**, a new approach called "Master curve approach" is developed for determining the effective stiffness of the 0^{o}-tow for any geometric parameters of the waviness. It is shown that the curve of the stiffness degradation for a given wavelength versus amplitudes can be considered as master curve for a 0^{o}-tow with different wavelength. A simple fitting expression can be found for the master curve considered for a small wavelength. The fitting expression contains only one unknown fitting constant which depends only on the elastic properties of the material.

In both approaches, it is demonstrated that the 90^{o}-tow's effective stiffness can be taken equal to the transverse properties of the unidirectional material without having significant error on the result of the NCF stiffness calculation using classical laminate theory and effective stiffness for the 0^{o}-tow determined either from the "Boundary Condition" approach or from the "Master Curve" approach.

3. References

[1] Varna J, Berglund LA. Mechanics of fiber composite materials-micromechanics, laminate theory and failure analysis. Division of Polymer Engineering. Luleå University of Technology.

[2] Mattsson D, Joffe R, Varna J. Damage in NCF composites under tension: effect of layer stacking sequence. Fracture of composite materials 2008; 75(9):2666-2682.

[3] Mattsson D. Mechanical performance of NCF composites. Doctoral thesis, Luleå University of Technology 2005.

[4] Carmisciano S, De Rosa IM, Sarasini F, Tamburrano A, Valente M. Basalt woven fiber reinforced vinylester composites: Flexural and electrical properties. Materials and design 2011; 32: 337-342.

[5] Hogg PJ, Ahmadnia A, Guild FJ. The mechanical properties of non-crimped fabric-based composites. Composites 1993; 24 (5): 423-432.

[6] Hogg PJ, Woolstencroft DH. Non-crimp thermoplastic composite fabrics: aerospace solutions to automotive problems. 7th Ann ASMIESD advanced composites conference Detroit 1991: 339-349.

[7] Mounitz AP, Leong KH, Herszberg I. A review of the effect of stitching on the in-plane mechanical properties of fiber-reinforced polymer composites. Composites Part A 1997; 28: 979-991.

[8] Mattsson D, Joffe R, Varna J. Methodology of characterization of internal structure parameters governing performance in NCF composites. Composites Part B: Engineering 2007; 38: 44-57.

[9] Barkanov E. Introduction to the finite element method. Institute of materials and structures, Faculty of civil engineering, Riga Technical University 2001.

[10] Ritz W. über eine neue metode zur lösung gewisser variations problem der matematischen physik. Journal für die reine und angewandte Mathematik 2009; 1909(135): 1-61.

[11] Tan P, Tong L, Steven GP. Modeling for predicting the mechanical properties of textile composites- a review. Composites Part A 1997; 28A: 903-922.

[12] Naik NK, Shembekar PS. Elastic behavior of woven fabric composites: I-Lamina analysis. Journal of composite materials 1992; 26: 2197-2225.

[13] Shembekar PS, Naik NK. Elastic behavior of woven fabric composites: II-Laminate analysis. Journal of composite materials 1992; 26: 2226-2246.

[14] Naik NK, Shembekar PS. Elastic behavior of woven fabric composites: III-Laminate design. Journal of composite materials 1992; 26: 2523-2541.

[15] Ishikawa T, Chou T. Elastic behavior of woven hybrid composites. Journal of composite materials 1982; 16: 1982, 2-19.

[16] Ishikawa T, Chou T. One dimensional micromechanical analysis of woven fabric composites. AIAAJ 1983; 21: 1714-1721.

[17] Ishikawa T, Chou T. Stiffness and strength behavior of woven fabric composites. Journal of material sciences 1982; 17: 3211-3220.

[18] Byström J, Jekabsons N, Varna J. An evaluation of different models for prediction of elastic properties of woven composites. Composites Part B 2000; 31: 7-20.

[19] Tessitore N, Riccio A. A novel FEM model for biaxial non-crimp fabric composite materials under tension. Computers and structures 2006; 84: 1200-1207.

[20] Drapier S, Wisnom MR. A finite element investigation of the interlaminar shear behavior of non-crimp-fabric-based composites. Composite science and technology 1999; 59: 2351-2362.

[21] Edgren F, Asp LE. Approximate constitutive model for non-crimp fabric composites. Composites Part A 2005; 36: 173-181.

[22] Mattsson D, Varna J. Average strain in fiber bundles and its effect on NCF composite stiffness. Journal of Engineering Materials and Technology 2006; 129: 211-219.

[23] Marklund E, Varna J, Asp LE. Modelling stiffness and strength of non-crimp fabric composites: semi-laminar analysis. Non-crimp fabric composites: manufacturing, properties and applications edited by Stepan V.Lomov 2011; 17: 402-438.

[24] Edgren F, Mattsson D, Asp LE, Varna J. Formation of damage and its effects on non-crimp fabric reinforced composites loaded in tension. Composites Science and Technology 2004; 64: 675-692.

Paper A

Effective stiffness of curved 0^o-layers for stiffness determination of cross-ply non-crimp fabric composites

H. Zrida[1,2], E. Marklund[1,3], Z. Ayadi[2] and J. Varna[1,*]

[1] *Division of Materials Science, Luleå University of Technology, SE-971 87 Luleå, Sweden*
[2] *Institut Jean Lamour, Ecole Européenne d'Ingénieurs en Génie des Matériaux, 6 Rue Bastien Lepage,*
F-54010 Nancy Cedex, France
[3] *Swerea SICOMP, SE-431 22 Mölndal, Sweden*
**Corresponding author (Janis.Varna@ltu.se)*

Abstract

The effect of the 0^o-tow waviness on axial stiffness of cross-ply non-crimp fabric (NCF) composites is analyzed using multiscale approach. The curved 0^o and 90^o-layers are represented by flat layers with effective stiffness properties and classical laminate theory (CLT) is used to calculate the macroscopic stiffness. The effective 0^o-layer stiffness is calculated analyzing isolated curved 0^o-layers subjected not only to end loading, but also to surface loads. The surface loads are identified in a detailed FE-analysis and approximated by a sinus shaped function with amplitude depending on the waves parameters. The sinus shaped surface loads are then applied to an isolated curved 0^o-layer FE-model together with end loading to calculate the effective stiffness of the layer. Finally, the effective 0^o-layer stiffness was successfully used to calculate the macroscopic stiffness of the composite proving validity of the approach being used and showing that, without losing accuracy, elastic properties in the 90^o-layers with bundle structure can be replaced by the transverse stiffness of the homogenized 90^o-layer material.

Keywords: Waviness, non-crimp fabric (NCF), boundary conditions, effective stiffness, classical laminate theory (CLT)

1. Introduction

Due to high material costs and sensitivity to out-of-plane loads (e.g. impact damage) of prepreg tape based composites, new manufacturing methods and material architectures based on dry preforms have been employed in the last decade producing civil aircraft primary structures. Non-crimp fabric (NCF) reinforced composites are particularly attractive due to their relatively high performance with less drop in in-plane properties compared to traditional woven architectures, reasonable cost and ease of handling during manufacture. As a result there is a strong interest among aircraft manufacturers and within other sectors such as wind energy and automotive industry, to use NCF based composites in primary structures.

NCF composites are manufactured from layered textile preforms consisting of fiber bundles with a certain orientation assembled by warp-knitted threads **[1]**. This production technique allows for substantial reductions in production costs compared to prepreg tape based materials. In addition improvements in damage tolerance as well as out-of-plane fracture toughness have been reported **[2-4]**. During composite manufacture, preforms are stacked in a mold and infiltrated by a thermoset resin to form the composite. Thus an NCF composite is created which is heterogeneous not only on microscale (fibers and resin) as for prepreg based composites, but also on mesoscale due to the appearance of distinct fiber bundles and resin pockets. The described heterogeneities on two very different length scales allow for homogenization of properties.

Ideally, NCF composites would consist of perfectly aligned fiber bundles where the size of each bundle is determined by the stitching procedure. However, due to the complex manufacturing technique, NCF composites have both in- and out-of-plane waviness of the bundles which reduces the in-plane stiffness. In **[5,6]** experimental data regarding the measured out-of-plane waviness are discussed, and the waviness in terms of sinusoidal shape was used in a 2D FE-model of a composite with periodic structure in the thickness direction and a biaxial NCF as a repeating unit cell (RUC) in order to study the effect of the parameters defining the 2D mesoscopic model on the NCF compressive strength. It has been shown that the NCF compressive strength is controlled by the 0^{o}-tow geometrical instability and by the resin shear plastic flow.

In the sense of the out-of-plane waviness the architecture of real NCF composite described above and shown in **Figure 1a** has similarities to woven fabric composites, see **Figure 1b**. Therefore, methods and theoretical models for woven fabric composites **[7]** have been applied also for NCF composites. For woven composites Ishikawa and Chou **[8, 9]** proposed the mosaic and fiber undulation models. In these models, an assumed representative volume element (RVE) is divided into infinitesimal strips and the classical laminate theory (CLT) is used to calculate elastic properties of the strip. The mosaic model disregards the waviness of the bundle whereas the fiber undulation model also includes the waviness. In **[10],** the 3D RVE consists of flat matrix pockets as well as in-plane and interlaced bundle regions. The iso-strain assumption was used in the in-plane directions and constant stress assumption in the out-of-plane direction.

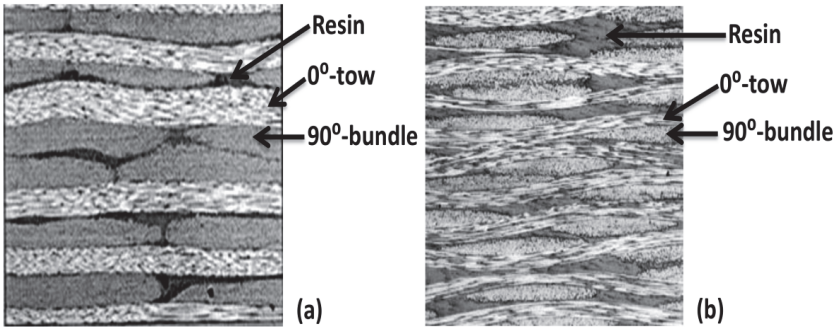

Figure1. Edge view of the mesostructure: **(a)** NCF composite **(b)** Woven composite

Similar analytical models have been applied to NCF composites in **[11, 12].** In **[13]** the stitching thread was included in the analysis. Stiffness expressions for NCF composites assembled by a warp knitting procedure were presented in **[14]** using the manufacturing parameters as input. In **[15]** the reduced volume fraction of the bundle and matrix due to the distortion created by the stitching yarn was analyzed. The reduced volume fraction was then used together with CLT to predict the mechanical properties of the laminate. Super-elements containing all details of the NCF architecture that necessarily requires numerical methods were introduced in **[16]**. More complex semi-analytical approaches are presented in **[17, 18]**.

A different approach is using the assumption that the NCF composite stiffness problem can be reduced to CLT problem for laminate with “effective” elastic properties of layers. The effective stiffness is calculated considering an isolated curved beam (bundle, layer), replacing its interaction with the rest of the composite with proper boundary conditions. In **[19]** the effective modulus was calculated using a Timoshenko model for curved beams with different boundary conditions during axial loading: “free beam” (no restrictions on z-displacement); “simple support” (zero z-displacement in support points); “elastic foundation” represented by one spring leading to very similar result as in case with “simple support”. The reduction of the effective bundle modulus was described by a knock-down factor.

Since the results were very sensitive with respect to the boundary conditions, we conclude that definition of surface conditions applied to curved tows to obtain effective stiffness representative for its behavior in the NCF composite remains an unresolved problem.

The main objective of the presented paper is to develop and validate CLT based methodology for axial stiffness calculation of imperfect biaxial NCF composites with fiber tow waviness. In this approach the curved tows/layers are replaced by straight ones with effective elastic properties. Isolated curved layers with appropriate boundaries and end conditions are suggested for effective properties determination. To identify what type of surface loads on the isolated curved 0^o-layer will represent its behavior in the NCF composite, FE-analysis of the stress/traction distributions at the 0^o-layer/90^o-layer interface in the NCF composite are conducted and sinus shaped functions are introduced to represent the surface load distribution. This approximation is then used in further numerical modeling to calculate the effective modulus of the curved 0^o-layer. It is demonstrated that a CLT based analytical model, in which the nominal/average thickness of the 90^o-layer, the effective stiffness of the curved 0^o-layer and the effective stiffness of the 90^o-layer with varying thickness are used, renders good accuracy.

It has to be noted that the observed trends and obtained results may be of relevance not only for NCF composites with 0^o-bundle waviness, but also for woven composites.

2. Theoretical background

One of the approaches to keep relative simplicity and at the same time to account for out-of-plane waviness of tows (referred to as "bundle waviness" or "curved bundle" in following) is based on the use of an "effective" straight bundle which has the effective in-plane stiffness of the curved bundle. In this approach the laminate is made of layers containing "effective" bundles. In the next step the "effective" bundle structure in a layer is replaced by homogenized material and CLT is used to find the macroscopic stiffness.

The CLT approach for calculating the axial stiffness of the NCF composites is very attractive due to its simplicity in application. For a symmetric and balanced laminate the macroscopic in-plane stress-strain relationship is

$$\sigma_1^{(av)} = Q_{11}^{(LAM)}\varepsilon_1 + Q_{12}^{(LAM)}\varepsilon_2 \qquad \textbf{Eq. (1)}$$

In **Eq. (1)** direction 1 is the axial (loading) direction. Focusing on the laminate axial stiffness element $Q_{11}^{(LAM)}$ we will perform FE numerical analysis for plane strain case $(\varepsilon_2 = 0)$. In this loading case $Q_{11}^{(LAM)}$ is obtained directly dividing the calculated axial average stress by the macroscopic strain applied. The average stress is axial force F_1 divided by nominal (average) thickness of the laminate h. Hence

$$Q_{11}^{(LAM)} = \frac{F_1}{h\varepsilon_1} \qquad \textbf{Eq. (2)}$$

The laminate stiffness elements are related to the *A*-matrix of the laminate

$$Q_{ij}^{(LAM)} = A_{ij}/h \qquad A_{ij} = \sum_{k=1}^{N} \bar{Q}_{ij}^{k}\, t_k \qquad \textbf{Eq. (3)}$$

With $\overline{Q}_{ij}^{k}$ and t_k being the effective stiffness matrix of the layer in global coordinates and average layer thickness respectively. Using the CLT approach with effective layers in a cross-ply NCF composite we obtain

$$Q_{11}^{(LAM)} = Q_{11}^{0-eff}\frac{t_0}{h} + Q_{22}^{90-eff}\frac{t_{90}}{h} \qquad \textbf{Eq. (4)}$$

Q_{22}^{90-eff} is the effective transverse stiffness of the homogenized 90°-layer with varying thickness (t_{90} is the average thickness), Q_{11}^{0-eff} is the effective axial stiffness of the curved 0°-layer. The problem now lies in the correct definition and determination of the effective stiffness.

3. FE modeling

3.1Materials

The fiber bundle and the homogenized layer are considered as unidirectional (UD) composites. Their elastic properties were calculated from the assumed fiber and matrix properties by using an FE-approach with hexagonal unit cell, as explained in **[20]**. In the bundle case the fiber volume fraction was *0.7*. In the homogenized layer the fiber volume fraction was always *0.6*. The constituent properties used and the homogenized layer elastic constants are given in **Table 1** for glass fiber and carbon fiber composites (GF/EP and CF/EP1). CF/EP2 composite properties were not calculated, they are assumed the same as for CF/EP1 except the longitudinal modulus which is lower (120GPa).

In calculations where the 90°-layer meso-structure with bundles (**Figure 2a**) was modeled, the shape of the 90°-bundle in **Figure 2a** was changed in order to keep the same fiber volume fraction $V_f = 0.6$ in the 90°-layer for models with different wave amplitudes and/or wave length.

Table1 elastic constants of constituents and homogenized layers

Constituents	E1 (GPa)	E2 (GPa)	v12	v23	G12 (GPa)	G23 (GPa)
Glass fiber	76.00	76.00	0.20	0.20	31.67	31.67
Carbon fiber	233.00	23.00	0.20	0.20	20.00	9.60
Epoxy resin	3.00	3.00	0.38	0.38	1.09	1.09
Composites	**E1 (GPa)**	**E2 (GPa)**	**v12**	**v23**	**G12 (GPa)**	**G23 (GPa)**
Carbon fiber/Epoxy (CF/EP1)	141.00	8.80	0.26	0.44	3.60	3.10
Glass fiber/Epoxy (GF/EP)	46.80	11.30	0.26	0.45	3.80	4.00
Cabon fiber/Epoxy (CF/EP2)	The same properties as CF/EP1 with lower modulus E1=120 GPa					

3.2Geometry

In previous studies (e.g. **[19]**) the 0^o-bundle waviness was assumed sinusoidal in two possible cases: the in- phase case, when the waves of the outer 0^o-layers are in phase, and out of phase case, when the waves of the outer 0^o-layers are out of phase. These are the extreme cases and the real geometry is somewhere in between. As a matter of fact in a real composite the RVE is often much larger than the wave length of the individual bundle in one blanket: the NCF composite consists of several blankets of the fabric with a possible random shift in the horizontal directions. Therefore simple repeating units are not a good composite representation either in the thickness or in the in-plane directions. If any, then a simple model, where the curved 0^o-layer and the neighboring 90^o-layer are shown explicitly (this is the analyzed unit) and the rest of layers is replaced by effective macro-material (laminate), could be acceptable to analyze trends of meso-scale stress distributions.

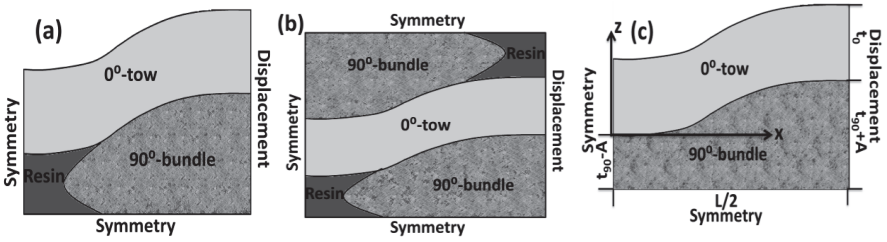

Figure2. NCF composites with **(a)** and **(b)** bundle structure and **(c)** homogenized 90^o-layer

Models in **Figure 2a** and **2b** represent a 0/90 unit on the NCF composite surface and inside the composite, respectively for a particular case of cross-ply NCF composite with zero shift between blankets. In this case the stiffness of the unit is the NCF composite stiffness and also the stress distributions are representative. **Figure 2a** may be also considered as an approximate representation of the top part of a more general NCF composite where response of the rest of the composite is replaced with symmetry conditions.

In this paper the focus is on the 0/90 unit at the composite surface as shown in **Figure 2a**. The thickness of the surface 0^o-layer is equal to the average thickness of the 90^o-layer, $t_0 = t_{90}$ .The top surface of the 0^o-layer is traction free. The model shown in **Figure 2c** represents the same unit but with homogenized 90^o-layer.

3.3 Mesh and boundary conditions

The analysis was conducted using the commercial FE software ANSYS14.0. PLANE42 elements with plane strain assumption were used. Two types of models were analyzed:

a) Individual curved 0^o-layer , see **Figure 3**
b) NCF composite shown in **Figure 2a** and waved laminate **Figure 2c**

The mesh was mapped so that each element's coordinate system in the 0^o-layer follows the sinusoidal shape of the layer. The area of each layer was meshed with quadratic elements with *200* divisions along the model length and *40* divisions along the thickness direction.

The boundary conditions are presented in **Figure 2 and Figure 3**. For all models, symmetry condition is applied along the left vertical boundary and an x-displacement is applied along the right vertical boundary. The average strain in x-direction introduced by the applied displacement is equal to *1%*. An additional symmetry condition was applied to the waved laminate along the bottom boundary which is the mid-plane of $[0, 90]_s$ NCF composite or the interface with the rest of the composite in a more general case.

An isolated sinusoidal 0^o-layer with constant thickness subjected to load in x-direction at ends and different combinations of loads on curved surfaces was also analyzed using FE (only half of the wavelength was considered). The boundary conditions used analyzing isolated curved 0^o-layers are shown in **Figure 3**. In addition, for the "free end" 0^o-layer, the displacement in the z-direction for the middle node of the left vertical boundary was set to zero. For the curved 0^o-layer with "fixed ends" the same displacement was zeroed for the first and the last nodes

along the bottom edge. For the 0^o-layer on "rigid foundation", this displacement is zero for all nodes belonging to the bottom boundary. Finally, for the model in **Figure 3d**, the load was distributed along the bottom surface of the curved 0^o-layer following a sinus shape function.

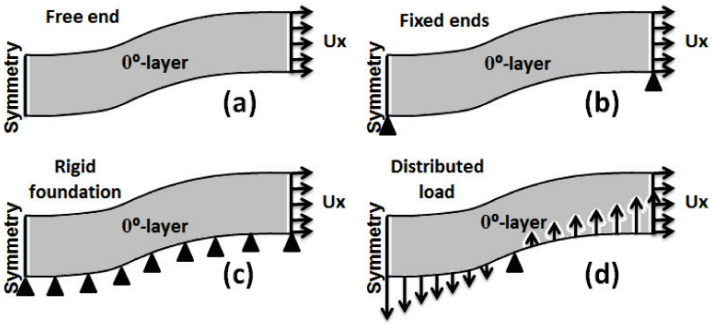

Figure3. Curved layer subjected to different boundary conditions

3.4 Meso-scale homogenization

An important step towards using CLT is replacing the bundle mesostructure of the layer with a homogenized layer. In **[18]** the axial stiffness of a flat layer with bundle mesostructure was analyzed showing that without losing accuracy, the mesostructure can be replaced by homogenized layer with elastic properties corresponding to the average volume fraction of fibers in the layer. The difference between the longitudinal modulus of the homogenized layer and the layer with bundle mesostructure is extremely small. This result is not surprising since rule of mixtures (RoM) is very accurate for longitudinal modulus). It justifies the use of curved 0^o-layer instead of curved 0^o-bundles in NCF composite stiffness investigation.

Here we will inspect the validity of the assumption that the bundle structure in the curved 90^o-layer can be replaced by a homogenized curved layer, in other words, we will compare the axial stiffness of models in **Figure 2a** and **Figure 2c**. In a similar investigation Mattson et al. **[18]** demonstrated that the mesoscale details on the NCF laminate stiffness can be neglected for the case with straight 0^o-bundles.

In calculations both models (**Figure 2a** and **Figure 2c**) have the same fiber content *0.6* in the 90°-layer and $t_0 = t_{90} = 0.3mm$. The change in the amplitude A of the waviness does not change the average thickness of the 90°-layer. It is equal to the thickness when there is no waviness. The z-coordinates of the points which belong to the interface are related to the x-coordinate as follows:

$$z = A\sin\left(\frac{2\pi}{L}\left(x - \frac{L}{4}\right)\right) = -A\left(cos\left(\frac{2\pi x}{L}\right)\right) \qquad \textbf{Eq. (5)}$$

The results in **Figure 4** for different combinations of amplitude and the wave length show that the stiffness is just marginally affected by the mesostructure of the bundles and the 90°-layer homogenization is justified. In the following only the model in **Figure 2c** is analyzed. The possible waviness of this layer is neglected because its effect on NCF composite axial modulus, studied here, is small.

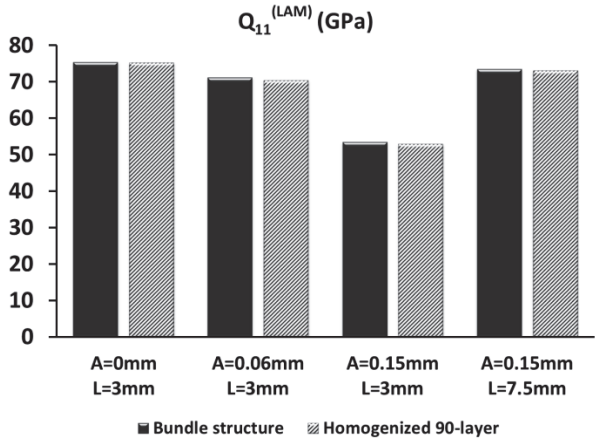

Figure4. Axial stiffness comparison between NCF composite with 90°-layers bundles and composite with homogenized 90°-layer

4. Numerical analysis

4.1Effect of wavelength and amplitude on laminate stiffness

Results for CF/EP1 laminate with elastic properties in **Table 1** are shown in **Figure5a.** Parameters A, t_0, L are defined in **Figure 2c**. In this figure t_0 is the thickness of the

curved 0^o-layer, t_{90} is the average thickness of the homogenized 90^o-layer, $h = t_0 + t_{90}$. It is clear that $Q_{11}^{(LAM)}$ is significantly reduced with increasing amplitude and decreasing wavelength of the waviness.

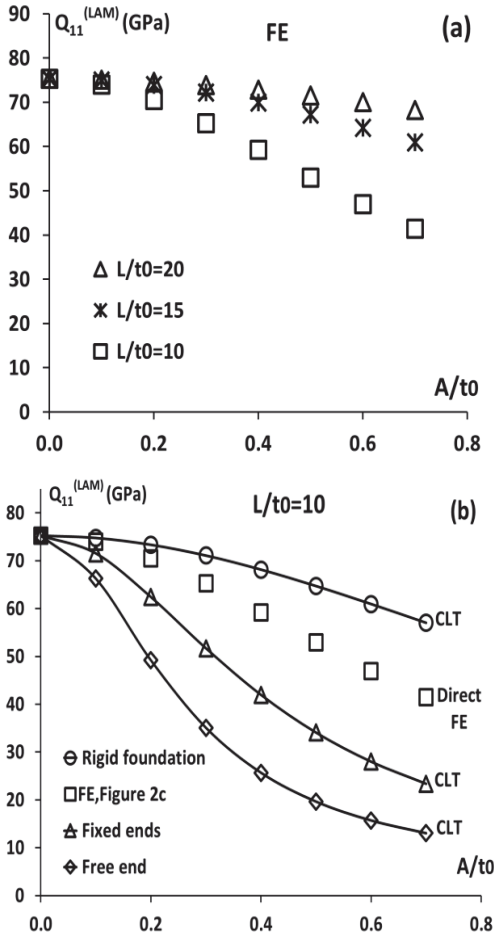

Figure5. Effect of the waviness on the CF/EP1 NCF composite axial stiffness ($t_0 = t_{90}^{(av)}$)**: (a)** Using the FE-model in **Fig 3c**; **(b)** CLT with effective stiffness of the curved layer according to different boundary conditions

One can see very large reduction of $Q_{11}^{(LAM)}$ with increasing amplitude and decreasing wavelength of the waviness.

4.2Predictions based on isolated curved layers

The three curves in **Figure5b** showing the laminate stiffness were obtained using **Eq. (4)**. The effective stiffness of the 0^o-layer Q_{11}^{0-eff} was calculated for isolated curved layer shown in **Figure 3** using FE with boundary conditions a), b) and c). The 90^o-layer effective stiffness was assumed equal to the 90^o-layer material transverse stiffness using data in **Table 1**. These curves may be compared with direct FE results (symbols in **Figure 5b**) taken from **Figure 5a**. The comparison demonstrates the failure of these boundary conditions used to give values of 0^o-layer effective stiffness relevant for using in **Eq. (4)**.

4.3Dependency of the effective stiffness of the layer on A/t_0 and L/t_0

The effective in-plane axial stiffness of the curved layer is lower than the stiffness of a straight layer mainly because the fibers are not oriented in-plane. However, as shown in **[19]**, the effective stiffness strongly depends also on the interaction with the adjacent material (tows of different orientations, resin).

Calculating $Q_{11}^{(LAM)}$ according to **Eq. (2)** we use the total force F_1 which due to force balance is the same in any cross-section. For example, in **Figure 2c** $F_1^R = F_1(x = L/2)$ is equal to $F_1^L = F_1(x = 0)$. In other words, using **Eq. (2)** and FE it is not important in which cross-section the reaction force is obtained before dividing it with the average composite thickness h .

If instead the CLT based **Eq. (4)** is used, the effective layer stiffness has to be found first. Similarly as was done for the whole laminate stiffness case, we would for this purpose divide the calculated force acting on some arbitrary cross-section of the layer by its cross-section area and then by the applied strain. However, the force on a cross-section of a layer depends on which cross-section we consider. For example

$$F_1^R(0°) \neq F_1^L(0°) \qquad F_1^R(90°) \neq F_1^L(90°) \quad F_1^R(0°) + F_1^R(90°) = F_1 \qquad \textbf{Eq. (6)}$$

The numbers $0°$ and $90°$ in parenthesis indicate the layer under consideration. Because of **Eq. (6)** effective layer stiffness calculated on the left and the right edge of the model differ

$$Q_{11}^{R}(0°) \neq Q_{11}^{L}(0°) \quad Q_{22}^{R}(90°) \neq Q_{22}^{L}(90°) \qquad \textbf{Eq. (7)}$$

where

$$Q_{11}^{R}(0°) = \frac{F_1^R(0°)}{\varepsilon_1 t_0} \qquad Q_{11}^{L}(0°) = \frac{F_1^L(0°)}{\varepsilon_1 t_0}$$

$$Q_{22}^{R}(90°) = \frac{F_1^R(90°)}{\varepsilon_1\,(t_{90}+A)} \qquad Q_{22}^{L}(90°) = \frac{F_1^L(90°)}{\varepsilon_1\,(t_{90}-A)} \qquad \textbf{Eq. (8)}$$

Due to interaction, layers are not subjected to uniaxial loading and strictly speaking the calculated numbers are not stiffness matrix elements. This explains the two different values. The situation will be similar analyzing isolated curved layers with traction boundary conditions. Therefore, it has to be clarified which layer stiffness Q_{11}^{0-eff} and Q_{22}^{90-eff} to be used in the CLT **Eq. (4)**.

For this purpose we may formally write that the force is distributed between 0^o-layer and 90^o-layer according to:

$$F_1^R = F_1^R(0°) + F_1^R(90°) \qquad \textbf{Eq. (9)}$$

$$F_1^L = F_1^L(0°) + F_1^L(90°) \qquad \textbf{Eq. (10)}$$

And

$$F_1^R = F_1^L = F_1 \qquad \textbf{Eq. (11)}$$

Averaging gives:

$$F_1 = \frac{F_1^R + F_1^L}{2} = \frac{F_1^R(90°)+F_1^L(90°)}{2} + \frac{F_1^R(0°)+F_1^L(0°)}{2} \qquad \textbf{Eq. (12)}$$

Substituting **Eq. (12)** in **Eq. (2)** and using **Eq. (8)**:

$$Q_{11}^{(LAM)} = \frac{Q_{22}^{R}(90)\frac{t_{90}+A}{t_{90}} + Q_{22}^{L}(90)\frac{t_{90}-A}{t_{90}}}{2}\frac{t_{90}}{h} + \frac{Q_{11}^{R}(0°)+Q_{11}^{L}(0°)}{2}\frac{t_0}{h} \qquad \textbf{Eq. (13)}$$

Comparing **Eq. (13)** with the CLT expression in **Eq. (4)** the correct expressions for effective stiffness of layers considering them as "isolated" is given by:

$$Q_{11}^{0-eff} = \frac{Q_{11}^{R}(0°)+Q_{11}^{L}(0°)}{2} \qquad \textbf{Eq. (14)}$$

$$Q_{22}^{90-eff} = \frac{Q_{22}^{R}(90)\frac{t_{90}+A}{t_{90}}+Q_{22}^{L}(90)\frac{t_{90}-A}{t_{90}}}{2} \qquad \textbf{Eq. (15)}$$

Forces for using in **Eq. (8)** were calculated from the model in **figure 2C** by summing the reaction forces acting on the nodes along the corresponding edge of the layer. The reaction force on the node shared by both layers is replaced by half of the reaction force of the neighboring node, by analogy with the reaction force on the upper-right node in the free upper boundary, which is also equal to half of the reaction force of its neighboring node. **Figure 6** shows how the effective stiffness of the 0°-layer,Q_{11}^{0-eff} and the effective stiffness of the 90°-layer Q_{22}^{90-eff} decrease due to the waviness described by A/t_0 for several values of L/t_0.The difference between $Q_{11}^{R}(0°)$ and $Q_{11}^{L}(0°)$ calculated on both edges is rather small. In contrast the transverse effective stiffness parameters of the 90°-layer, $Q_{22}^{R}(90)$ and $Q_{22}^{L}(90)$ have very different trends: one (calculated at $x = 0$) is increasing, the other one is decreasing. The combined effective stiffness Q_{22}^{90-eff} calculated according to **Eq. (15)** decreases from about 9 GPa to 7 GPa.

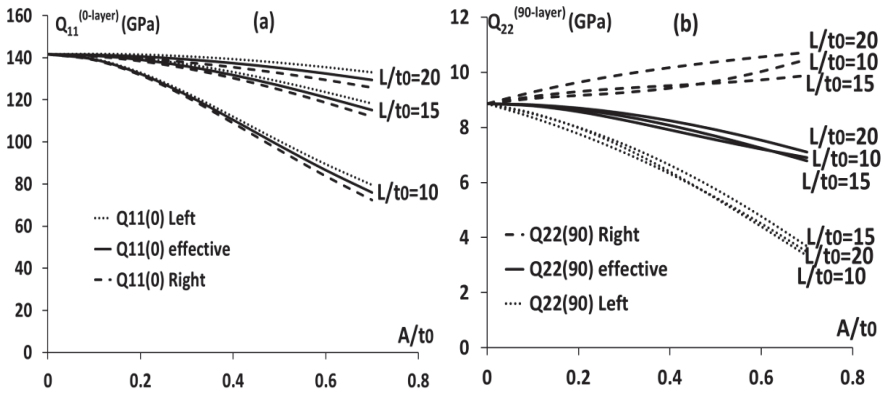

Figure6. Axial stiffness for **(a)** the 0°-layer and **(b)** the 90°-layer, CF/EP1 composite

We can introduce knock down factors for the laminate and the layers by dividing the effective stiffness with the stiffness corresponding to a reference case having straight tows (*A=0*). **Figure7** shows for CF/EP1 that for $L/t_0=10$ the decrease in composite stiffness is nearly the same as for the 0^o-layer effective stiffness.

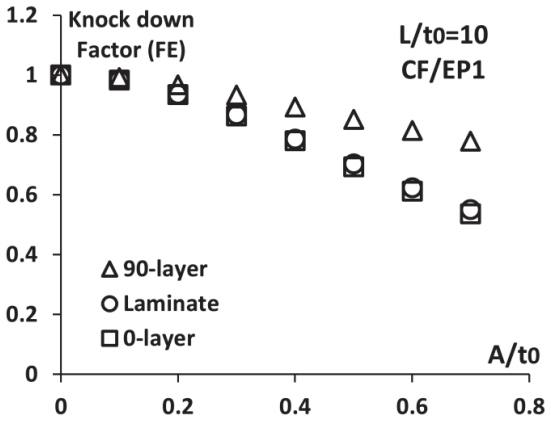

Figure7. Comparison between knock down factor of the 0^o-layer, the 90^o-layer and the laminate

Apparently the laminate stiffness reduction is dominated by the reduction of the 0^o-layer stiffness due to waviness. A simplified form of the laminate stiffness expression, **Eq. (4)**, in which the 90^o-layer effective stiffness is assumed equal to the 90^o-layer material stiffness may be therefore be motivated:

$$Q_{22}^{90-eff} = Q_{22}^{90} \qquad \textbf{Eq. (16)}$$

The accuracy of the simplification in **Eq. (16)** will be verified in following calculations.

4.4Approximation of tractions at the 0/90-layer interface

In line with the objectives of this study, the task is to find the effective stiffness of the curved 0^o-layer analyzing an isolated curved layer subjected to relevant boundary conditions. These include not only end loads applied to the layer, but also surface loading shown as "distributed load" in **Figure 3.** Only in the presence of "distributed load" forces $F_1^R(0°)$ and $F_1^L(0°)$ may differ.

Knowledge regarding the distributed load is conveniently obtained by analyzing stresses at the 0^o- and the 90^o-layer interface using FE. The results and the observed trends used to define shape functions for the interface stresses from fitting a limited number of FE-calculations are presented in this section. The methodology suggested for finding coefficients in these shape functions is described in more detail in Appendix. These functions can then be used for curved 0^o-layer stiffness analysis with an arbitrary amplitude or wavelength.

Local stress distribution at the 0/90-layers interface has been analyzed: The normal stress σ_n and the shear stress σ_{nt} were determined in each node along a path on the interface. In the FE-analysis those stress components are slightly different on both sides of the interface. The value along the path on the interface which is given by the code is the average of the stresses calculated for the closest element to the interface in the 0^o-layer and in the 90^o-layer. In **Figure 8**, the normal stress σ_n is plotted as a function of the normalized distance along the x-axis for different A/t_0 and L/t_0. The curves show large variation of the normal stress along the interface. This stress is equal to zero when there is no waviness. The waviness contributes to the appearance of tensile normal stress in the left part and compressive normal stress in the right part on the interface. The maximum value of the tensile and the compressive normal stress is increasing with decreasing L/t_0 and with increasing A/t_0. For simplicity, this behavior was fitted with a sinusoidal function, **Eq. (17)**, with amplitude depending on the waviness parameters and the elastic properties of the material.

$$\sigma_n = \sigma_{n0} sin\left(\frac{2\pi}{L}\left(x - \frac{L}{4}\right)\right) = -\sigma_{n0}\left(cos\left(\frac{2\pi x}{L}\right)\right) \; With \; \sigma_{n0} = f\left(\frac{A}{t_0}, \frac{L}{t_0}, E_1, etc\right) \textbf{ Eq. (17)}$$

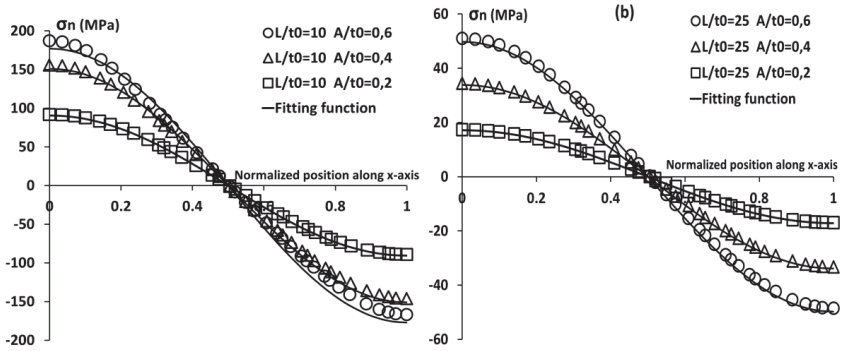

Figure 8. Normal stresses at layer interface in CF/EP1 composite and **fitting (a)** for L/t_0*=10*; **(b)** for L/t_0*=25*, applied strain *1%*.

In **Figure 9**, the shear stress σ_{nt} on the interface is plotted as a function of the normalized position along the x-axis for different A/t_0 and L/t_0. In a straight layer cross-ply laminate this stress component would be equal to zero. However, the rather complex σ_{nt} behavior becomes significant with increasing 0^o-layer amplitude. Calculations on isolated curved layers showed that the significance of the applied shear stress on the boundary is small (most important is the normal stress σ_n), justifying the use of the same rough sinus function approximation to fit the shear stress in the whole parameter region

$$\sigma_{nt} = \sigma_{nt0}\, sin\left(\frac{2\pi}{L}\left(x - \frac{L}{4}\right)\right) = -\sigma_{nt0}\left(cos\left(\frac{2\pi x}{L}\right)\right) \; With \;\; \sigma_{nt0} = f\;\left(\frac{A}{t_0}, \frac{L}{t_0}, E_1, etc\right) \textbf{ Eq. (18)}$$

As one can see in **Figure 9a** the fitting is obviously not good for *small* L/t_0 and sufficient for *larger* L/t_0 (**Figure 9b**).

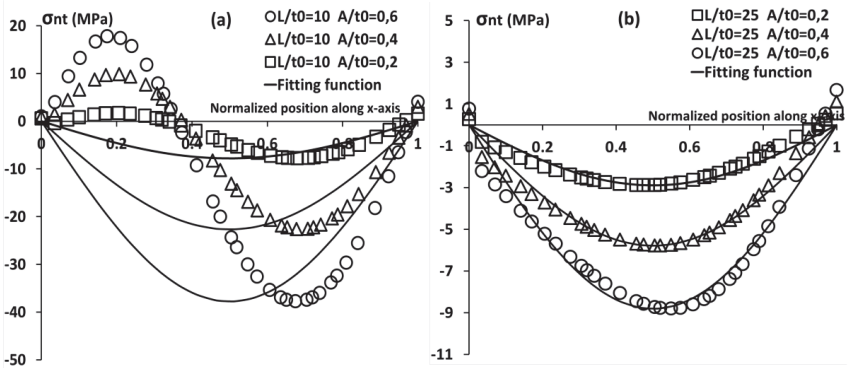

Figure 9 Shear stresses at layer interface in CF/EP1 composite and fitting **(a)** for L/t_0=10; **(b)** for L/t_0=25, applied strain *1%*.

Thus, performing FE-calculations for a limited number of L/t_0 and A/t_0 cases we can find approximate interface stress expressions for a given material to be used for any practical combination of these geometrical parameters.

The main objective of this part was to find simple expressions for further analytical application. The expressions for σ_{n0} and σ_{nt0} dependence on L/t_0 and A/t_0 are given in **Appendix**.

4.5Composite stiffness based on effective stiffness of an isolated 0^o-layer with surface loads

In this subsection we use the calculated and approximated normal and shear stress distributions along the layer interface as surface loads in an isolated curved 0^o-layer model shown in **Figure 10.** The approximate expressions for the normal and the shear stresses given in Appendix are used. The surface load is obtained by multiplying the stress components by the element length which is assumed equal to the distance dx between two neighboring nodes. The calculated load is applied in the local coordinate system related to each element on the bottom surface of the curved layer. This new boundary condition is introduced in addition to the symmetry on the left edge and the displacement applied in the right edge. Since the loading applied to the 0^o-layer is not uniaxial the Q_{11}^{0-eff} calculated using **Eq. (14)** is, strictly speaking,

not the axial stiffness. Nevertheless, it represents the curved 0^o-layer mechanical behavior in the composite.

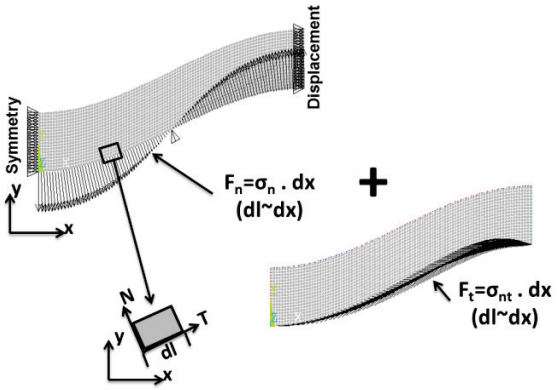

Figure10. Application of distributed load on the 0^o-layer surface

In **Figure 11,** where the calculated effective stiffness of an isolated 0^o-layer is presented together with the effective stiffness of the 0^o-layer determined from the waved cross ply laminate, see **Section 4.3**, good agreement between both solutions is demonstrated. For the sake of comparison, effective 0^o-layer stiffness calculated using the rest of boundary conditions in **Figure 3** is also presented. Effective stiffness in the case of fixed/free ends is unrealistically low, while rigid foundation is too high. The most accurate results are given by the beam with distributed surface load. Thus, the assumption of replacing the interaction between the 0^o and the 90^o-layers in the laminate by a distributed load applied to the curved beam is validated. The accuracy can be improved by more accurate fitting of the interface stresses; the simplicity can be improved by more rough approximation that, probably, would not affect the calculated stiffness too much.

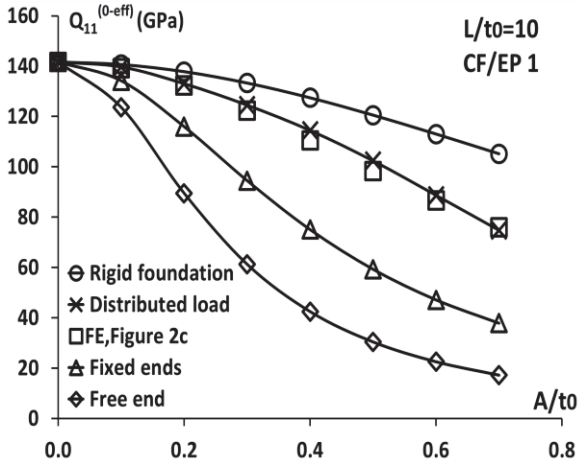

Figure11. Effective stiffness of the 0^o-layer with different boundary conditions

Finally, CLT, see **Eq. (4)**, is used to determine the laminate stiffness utilizing the effective stiffness of the curved 0^o-layer with distributed load, and the effective stiffness of the 90^o-layer. Effective 90^o-layer stiffness is used in two approximations: a) With varying thickness with values from **Figure 6b** (this requires FE calculations of the cross-ply composite); b) using **Eq. (16)**, i.e. $Q_{22}^{90-eff} = Q_{22}^{90}$ (which is not accurate, but simple for use). In **Figure 12** to **Figure 14** the laminate stiffness is presented as a function of A/t_0 for different L/t_0. In **Figure 12a**, **13a** and **14a** the effective stiffness of the 90^o-layer is used whereas in **Figures 12b**, **13b** and **14b** the 90^o-layer with varying thickness is represented by its transverse stiffness Q_{22}^{90} calculated using data in **Table 1**.These results show good agreement between the analytical CLT approach with the effective stiffness of the 0^o-layer and FE calculation of the laminate stiffness. Very small differences in results are seen when the 90^o-layer effective stiffness is represented by its material transverse stiffness, proving that this approximation may be used.

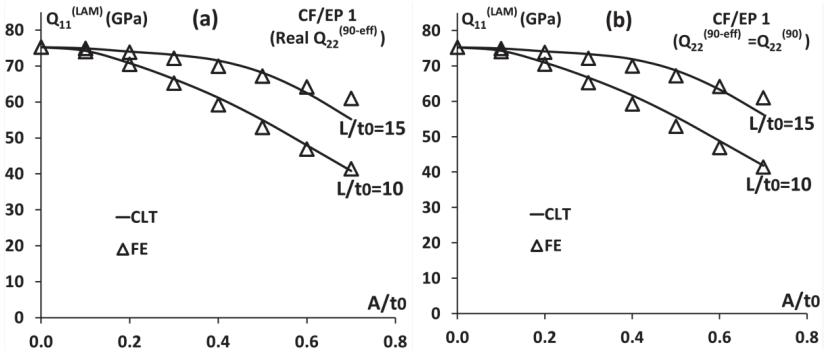

Figure12. CLT using effective stiffness compared to FE-analysis for CF/EP1

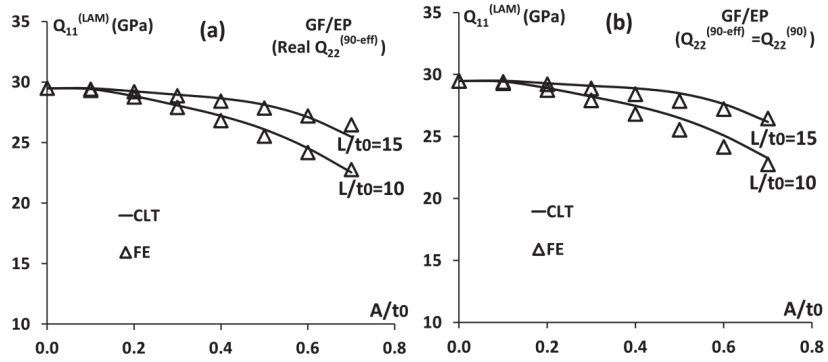

Figure13. CLT using effective stiffness compared to FE-analysis for GF/EP

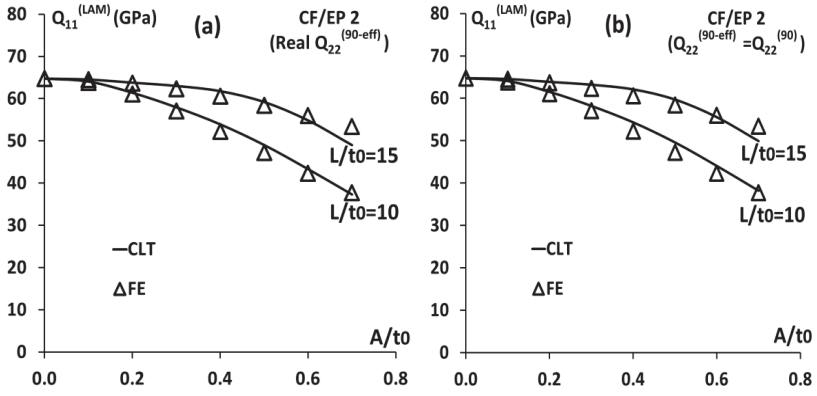

Figure14. CLT using effective stiffness compared to FE-analysis for CF/EP2

5. Conclusions

The effect of the 0^o-bundle waviness on stiffness of cross-ply NCF composites was modeled. Multiscale approach was used by first calculating the homogenized bundle material properties from its constituents by using an assumed hexagonal fiber packing. The bundle structure of the curved 0^o-layer and the bundle structure of the 90^o-layer with varying thickness are then replaced with homogenized materials. Finally, the curved 0^o-layer and the 90^o-layer with varying thickness were replaced by flat layers with effective stiffness and classical laminate theory was used to calculate the macroscopic stiffness. The presented paper focused on the axial macroscopic stiffness.

The macroscopic axial stiffness was expressed through the effective stiffness of the curved 0^o-layer and the effective stiffness of the 90^o-layer with varying thickness. It was shown that the effective stiffness of a layer in the composite can be calculated averaging the apparent stiffness, which are on the right and the left edges of the layer. These two forces to layer are different due to varying layer thickness and due to the interaction between layers resulting in normal and shear stresses at the 0/90-layer interface.

Using this approach the effective 0^o-layer stiffness was calculated analyzing isolated curved 0^o-layer subjected not only to end loading, but also to surface loading. To identify the surface loads to be applied, a detailed FE-analysis of the interface stresses was performed. It is concluded that these stresses can be approximated by a sinus shaped function with amplitude dependent on the wave length and amplitude of the curve normalized with respect to the layer nominal thickness. Fitting expressions for the stress amplitude dependence on these layer waviness parameters were obtained, and are given in Appendix.

The described sinus shaped surface loads were applied to isolated curved 0^o-layer FE-model together with end loading showing that the calculated effective stiffness of the layer is in good agreement with the effective stiffness of the 0^o-layer extracted from the cross-ply composite analysis. This proves that further efforts are

meaningful to develop analytical approximate models for curved beams with sinusoidal surface tractions.

Finally, the calculated effective 0-layer stiffness was successfully used to calculate the macroscopic stiffness of three different composites proving validity of the used multiscale approach. It was also shown that without losing accuracy the effective stiffness of the 90^o-layer (which generally speaking should be calculated numerically considering 90^o-layer with varying thickness and applied surface and end loads) can be replaced by the transverse stiffness of the homogenized 90^o-layer material.

Acknowledgements

It is gratefully acknowledged that the work performed in this paper is partly funded by the Swedish 5th National Aeronautical Research Program (NFFP5) through the project ReFACT, and also through the Joint European Doctoral Program in Material Science and Engineering (DocMase).

Appendix A

Interface stress amplitude approximate dependence on A/t_0 and L/t_0

Fitting the interface normal and shear stress with **Eq. (17)** and **Eq. (18)** respectively, the stress amplitudes σ_{n0} and σ_{nt0} are found. The monotonously decreasing values were fitted with the following function

$$\sigma_{n0}(Pa) = \frac{1}{C_{1n}+C_{2n}\left(\frac{L}{T}\right)+C_{3n}\left(\frac{L}{T}\right)^2} \qquad \textbf{Eq. (A.1)}$$

Constants determined by fitting

$$C_{2n} = C_{21n} + C_{22n}\left(\frac{A}{T}\right) + C_{23n}\left(\frac{A}{T}\right)^2 \qquad \textbf{Eq. (A.2)}$$

$$C_{3n} = B_n\left(\frac{A}{T}\right)^{-\alpha} \qquad \textbf{Eq. (A.3)}$$

The determined values of constants $C_{1n}, C_{21n}, C_{22n}, C_{23n}, B_n,\ \alpha$ for layers made of composite materials CF/EP1, CF/EP2 and GF/EP are given in **Table A.1**.

Table A.1 Values of constants for fitting maximum value of the interface normal stress ($\varepsilon_1 = 1\%$)

Material	C_{1n}	$C_{2n} = C_{21n} + C_{22n}\left(\frac{A}{T}\right) + C_{23n}\left(\frac{A}{T}\right)^2$			$C_{3n} = B_n\left(\frac{A}{T}\right)^{-\alpha}$	
		C_{21n}	C_{22n}	C_{23n}	B_n	α
CF/EP1	$5.200 \cdot 10^{-9}$	$-4.413 \cdot 10^{-10}$	$-2.612 \cdot 10^{-10}$	$7.900 \cdot 10^{-10}$	$2.337 \cdot 10^{-11}$	0.9339
CF/EP2	$5.400 \cdot 10^{-9}$	$-4.205 \cdot 10^{-10}$	$-3.707 \cdot 10^{-10}$	$8.993 \cdot 10^{-10}$	$2.682 \cdot 10^{-11}$	0.9364
GF/EP	$7.330 \cdot 10^{-9}$	$-2.609 \cdot 10^{-10}$	$-1.487 \cdot 10^{-9}$	$2.009 \cdot 10^{-9}$	$6.704 \cdot 10^{-11}$	0.9423

Amplitudes of shear stress are also fitted using the same type of expression:

$$\sigma_{nt0}(Pa) = \frac{1}{C_{1nt} + C_{2nt}\left(\frac{L}{T}\right) + C_{3nt}\left(\frac{L}{T}\right)^2} \qquad \textbf{Eq. (A.4)}$$

Parameters C_{1nt} , C_{2nt} and C_{3nt} are described by following functions:

$$C_{1nt} = C_{11nt} + C_{12nt}\ \exp(-C_{13nt}\frac{A}{T}) \qquad \textbf{Eq. (A.5)}$$

$$C_{2nt} = C_{21nt} + C_{22nt}\ \exp(-C_{23nt}\frac{A}{T}) \qquad \textbf{Eq. (A.6)}$$

$$C_{3nt} = C_{31nt} + C_{32nt}\ \exp(-C_{33nt}\frac{A}{T}) \qquad \textbf{Eq. (A.7)}$$

The constants for layers made of the different composite materials found by fitting are given in **Table A.2**.

Table A.2 Values of constants for fitting maximum value of the interface shear stress ($\varepsilon_1 = 1\%$)

Constants	CF/EP1	CF/EP2	GF/EP
$\mathbf{C_{11nt}}$	$1.261 \cdot 10^{-8}$	$1.577 \cdot 10^{-8}$	$-1.074 \cdot 10^{-8}$
$\mathbf{C_{12nt}}$	$-1.316 \cdot 10^{-6}$	$-7.652 \cdot 7$	$-9.064 \cdot 10^{-8}$
$\mathbf{C_{13nt}}$	5.200	4.163	4.229
$\mathbf{C_{21nt}}$	$6.325 \cdot 10^{-10}$	$1.121 \cdot 10^{-9}$	$3.984 \cdot 10^{-9}$
$\mathbf{C_{22nt}}$	$2.433 \cdot 10^{-7}$	$1.513 \cdot 10^{-7}$	$3.107 \cdot 10^{-8}$
$\mathbf{C_{23nt}}$	5.880	5.065	5.356
$\mathbf{C_{31nt}}$	$1.124 \cdot 10^{-10}$	$8.364 \cdot 10^{-11}$	$-4.166 \cdot 10^{-11}$
$\mathbf{C_{32nt}}$	$-6.445 \cdot 10^{-9}$	$-3.716 \cdot 10^{-9}$	$-2.616 \cdot 10^{-10}$
$\mathbf{C_{33nt}}$	6.180	5.205	4.568

References

[1] Leong KH, Ramakrishna S, Huang ZM, Bibo GA. The potential of knitting for engineering composites- a review. Composites Part A 2000; 31: 197-220.

[2] Dransfield K, Baillie C, Yiu-Wing M. Improving the delamination resistance of CFRP by stitching – a review. Composite Science and Technology 1994; 50: 305-317.

[3] Dransfield K, Jain L, Mai Y-W. On the effects of stitching in CFRPs- I. Mode I delamination toughness. Composite Science and Technology 1998; 58: 815-827.

[4] Jain L, Dransfield K, Mai Y-W. On the effects of stitching in CFRPs- II. Mode II delamination toughness. Composite Science and Technology 1998; 58: 829-837.

[5] Drapier S, Wisnom MR. Finite-element investigation of the compressive strength of non-crimp-fabric based composites. Composite Science and Technology 1999; 59: 1287-1297.

[6] Drapier S, Wisnom MR. A finite-element investigation of the interlaminar shear behaviour of non-crimp-fabric-based composites. Composite Science and Technology 1999; 59: 2351-2362.

[7] Miller AJ. The effect of microstructural parameters on the mechanical properties of non-crimp fabric composites. M.Ph. thesis Cranfield University School of Industrial and Manufacturing Science 1996.

[8] Ishikawa T, Chou TW. Elastic behaviour of woven hybrid composites. Journal of Composite Materials 1982; 16: 2-19.

[9] Ishikawa T, Chou TW. One-dimensional micromechanical analysis of woven fabric composites. AIAA 1983; 21(12): 1714-1721.

[10] Kurath P, Karayaka M. Deformation and failure behaviour of woven Composite Laminates. Journal of Engineering Materials and Technology 1994; 116: 222-232.

[11] Wang Y, Li J, Do PB. Properties of composites laminates reinforced with E-glass multiaxial non-crimp fabrics. Journal of Composite Materials 1995; 29(17): 2317-2333.

[12] Bibo GA, Hogg PJ, Kemp M. Mechanical characterisation of glass- and carbon-fibre-reinforced composites made with non-crimp fabrics. Composite Science and Technology 1997; 57(9-10): 1221-1241.

[13] Chun HJ, Ryu KS, Byun JH. Predictions of Elastic Properties of Multi-axial Warp Knitted Fabric Composites. Key Engineering Materials 2004; 261-263(II): 1499-1504.

[14] Robitaille F, Clayton BR, Long AC, Souter BJ, Rudd CD. Geometric modelling of industrial preforms: warp-knitted textiles. Proceedings of the Institution of Mechanical Engineers Part L, Journal of Materials: Design and Applications 2000; 214: 71-90.

[15] Klopp K, Veihelmann B, Kolkmann A, Laourine E, Gries T. Use of reinforcement textiles in fiber reinforced plastics. Tech Text 2003; 46: 59-63.

[16] Tessitore N, Riccio A. A novel FEM model for biaxial non-crimp fabric composite materials under tension. Computers and Structures 2006; 84: 1200-1207

[17] Byström J, Jekabsons N and Varna J. An evaluation of different models for prediction of elastic properties of woven composites. Composites Part B 2000; 31:7-20.

[18] Mattsson HD, Varna J. Average strain in fibre bundles and its effect on NCF composite stiffness. Journal of Engineering Materials and Technology 2007; 129: 211-219.

[19] Edgren F, Asp LE. Approximate analytical constitutive model for non-crimp fabric composites. Composites Part A 2005; 36: 173-181.

[20] Marklund E, Asp LE, Varna J. Modelling stiffness and strength of non-crimp fabric composites semi-laminar analysis. In: Stepan VL editor. Woodhead publishing in materials,Non-crimp fabric composites: manufacturing, properties and application 2011. 403-438.

Paper B

Master curve approach to axial stiffness calculation of biaxial composites with bundle waviness

H. Zrida[1,2], E. Marklund[1,3], Z. Ayadi[2] and J. Varna[1,*]

[1] *Division of Materials Science, Luleå University of Technology, SE-971 87 Luleå, Sweden*
[2] *Institut Jean Lamour, Ecole Européenne d'Ingénieurs en Génie des Matériaux, 6 Rue Bastien Lepage,*
F-54010 Nancy Cedex, France
[3] *Swerea SICOMP, SE-431 22 Mölndal, Sweden*
**Corresponding author (Janis.Varna@ltu.se)*

Abstract

The effect of 0^o-tow out-of-plane waviness on the biaxial Non-Crimp-Fabric (NCF) composite axial stiffness is investigated. Homogenizing, the bundle mesostructure of the NCF composite is replaced by layers. Then the composite is represented by a laminate with flat layers with effective stiffness properties representing the curved 0^o-layer and the 90^o-layer with varying thickness. It is shown that the NCF composite knock-down factor characterizing the stiffness degradation has almost the same dependence on wave parameters as the knock-down factor for the curved 0^o-layer. Numerical analysis showed that 90^o-layer knock-down factor versus amplitude curves for different wavelength can be reduced to one master curve which can be described by a one-parameter expression with the parameter dependent on the used material. This observation is used to obtain high accuracy for analytical predictions for knock down factors for cases with different wavelength and amplitudes based on two FE calculations only.

Keywords: Waviness, knock-down factor, stiffness, master curve, classical laminate theory (CLT)

1. Introduction

New manufacturing methods and material architectures had been employed over the last decade using dry woven or Non Crimp Fabric (NCF) preforms with following resin infusion. NCF based composites ideally would have in-plane stiffness similar to

prepreg tape composites. In addition, improvements in damage tolerance as well as out-of-plane fracture toughness have been reported **[1-3]**. That's why the interest in the wind energy and car industry as well as among European aircraft manufacturers to use NCF based composites in primary structures is so strong.

NCF composites are manufactured from layered textile preforms consisting of fiber bundles with a certain orientation assembled by warp-knitted threads **[4]**. Thus a NCF composite is heterogeneous not only on fiber/matrix scale as prepreg tape based composites, but also on mesoscale (impregnated fiber bundles and resin pockets). Since the bundle scale is much larger than the fiber scale, homogenization over the fiber/matrix scale is possible representing the bundle as transversally isotropic material.

Ideally, NCF composites would consist of perfectly aligned fiber bundles where the size of each bundle is determined by the stitching procedure. However, NCF composites have both in- and out-of-plane waviness of the bundles which reduces the in-plane stiffness. The out-of-plane waviness was measured in **[5,6]**. A sinusoidal shape of the waviness was assumed and used in a two-dimensional finite element model (FE) of the composite that had periodic structure in the thickness direction with a bi-axial non-crimp fabric as a repeating unit cell.

Assuming periodic out-of-plane waviness the architecture of NCF composite has similarities to woven fabric composites and therefore methods and models for woven fabric composites **[7]** have been applied for NCF composites as well. For woven composites Ishikawa and Chou **[8, 9]** proposed the mosaic and fiber undulation models. The mosaic model disregards the waviness of the bundle whereas the fiber undulation model also includes the waviness. For example in **[10]**, the 3-D representative volume element (RVE) consists of flat matrix pockets as well as in-plane and interlaced bundle regions. The iso-strain assumption was used in the in-plane directions and constant stress assumption was used in the out-of-plane direction. Similar models have been applied to NCF composites in **[11, 12].** In **[13]** the stitching tread was included in the analysis. Stiffness expressions for NCF

composites assembled by a warp knitting procedure were presented in **[14]** using the manufacturing parameters as input. In **[15]** the reduced volume fraction of the bundle and matrix due to the distortion created by the stitching yarn was analyzed. The reduced volume fraction was then used together with CLT to predict the mechanical properties of the laminate. Super-elements containing all details of the NCF architecture that necessarily requires numerical methods were introduced in **[16]**. More complex semi-analytical approaches are presented in **[17, 18]**.

Another group of models relies on classical laminate theory (CLT) using assumption that the curved bundle with out-of plane waviness can be replaced by "effective" flat layer. In **[19]** the effective modulus was calculated using analytical Timoshenko model for curved beam, applying several boundary conditions in thickness (z) direction during axial loading: "free beam" (no restrictions on z-displacement); "simple support" (zero z-displacement in support points); "elastic foundation" represented by one spring leading to very similar result as in the case with "simple support". The reduction of the effective bundle modulus was described by a knock-down factor. The results were not satisfactory and in **[20]** a detailed FE-analysis was performed finding that the loads on the tow surface have to be accounted for. For sinus-shaped tow they can be described by sinus function with amplitude dependent on the wave length and amplitude of the curve.

In the presented paper we are demonstrating that the axial stiffness of biaxial cross-ply NCF composite described by knock-down factor is almost the same as the knock down factor for the curved layer stiffness obtained in the same FE calculation. Then a novel "master curve approach" is presented which allows calculating the knock down factor of curved layer of arbitrary wave amplitude and length. The master curve for the given NCF composite material is obtained fitting FE knock-down factor values for one (preferably relatively short) wavelength and at least two values of amplitude. Only one additional FE calculation is required to cover all possible amplitude cases for a different wavelength. The curved layer knock-down factor is used to calculate the NCF composite knock-down factor. The very high accuracy of this approach is demonstrated in comparison with direct FE calculations.

2. Homogenization

In a previous study **[19]** a two blanket cross-ply NCF's 0^o-tow waviness was assumed sinusoidal and two possible geometrical configurations were analyzed numerically: the in-phase case, when the waves of the two outer 0^o-layers are in phase, and the out-of-phase case, when the waves of the outer 0^o-layers are out of phase. These are the extreme cases and in a real composite the RVE is often much larger than the wave length of the individual bundle in one blanket because the blankets of the fabric are randomly shifted in horizontal directions. In this paper we analyze the stiffness of a simple 0/90 unit of the NCF composite. The rest of the composite is roughly replaced with symmetry condition. Two units are analyzed, a unit with a surface 0^o-layer, see **figure 1a** and **1b**, and another with an embedded 0^o-layer, see **figure 1c**. The units correspond to a particular case of cross-ply NCF composite with zero shifts between blankets.

Bundles in the NCF composite are considered as unidirectional (UD) composites with certain fiber volume fraction and their elastic properties may be calculated using hexagonal unit cell as it was explained in **[21]** or simple rule of mixture based on iso-strain assumption, Halpin-Tsai expressions etc.

Bundles or layers with out-of-plane waviness are referred in following as "curved bundles" or "curved layers". First we assume that the structure of curved bundles in a layer may be replaced by homogenized layer with average fiber content which was kept 0.6 in the current investigation. The elastic constants of the layers and the constituents are given in **Table 1** for glass fiber- and carbon fiber- epoxy composites (GF/EP and CF/EP).

Table1 Elastic constants of constituents and homogenized layers

Constituents	E1 (GPa)	E2 (GPa)	v12	v23	G12 (GPa)	G23 (GPa)
Glass fiber	76.00	76.00	0.20	0.20	31.67	31.67
Carbon fiber	233.00	23.00	0.20	0.20	20.00	9.60
Epoxy resin	3.00	3.00	0.38	0.38	1.09	1.09
Composites	**E1 (GPa)**	**E2 (GPa)**	**v12**	**v23**	**G12 (GPa)**	**G23 (GPa)**
Carbon fiber/Epoxy (CF/EP)	141.00	8.80	0.26	0.44	3.60	3.10
Glass fiber/Epoxy (GF/EP)	46.80	11.30	0.26	0.45	3.80	4.00

The error introduced by replacing the layer with bundles by homogenized layer was analyzed before, for example, in **[18]** showing that the axial stiffness of a flat 0^o-layer does not change if the bundle mesostructure of the 0^o-layer is replaced by homogenized layer with elastic properties corresponding to the average volume fraction of fibers in the layer. This result justifies the use of curved 0^o-layer instead of curved 0^o-bundles in NCF composite stiffness investigation. The same study **[18]** demonstrated that the 90^o-layer meso-scale details on the NCF laminate stiffness can be neglected in cross-ply NCF with straight 0^o-bundles and constant 90^o-layer thickness. The validity of the assumption that in NCF composite with curved 0^o-layer the 90^o-layer bundle structure can be homogenized ("smeared out") was checked in **[20]** comparing axial stiffness of models in **figure 1a** and **figure 1b** with sinusoidal shape of the waviness.

In calculations both models had the same fiber content. Changing the amplitude A of the waviness the average thickness of the 90^o-layer was not changed. The results showed that the stiffness is just marginally affected by the mesostructure of the bundles and the 90^o-layer homogenization is justified.

In the next step we adapt the CLT approach to NCF composite stiffness calculation replacing the curved layer with a straight layer which has the "effective" in-plane stiffness of the curved layer. Thus, the laminate is made of "effective" layers.

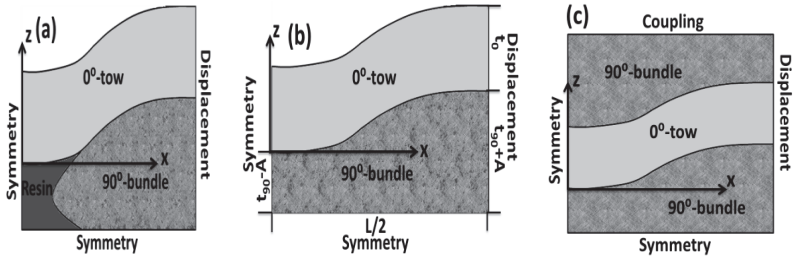

Figure1. NCF composites units **(a)** surface 0^o-layer with bundle structure **(b)** surface 0^o-layer with homogenized 90^o-layer **(c)** embedded 0^o-layer with homogenized 90^o-layers.

3. Theoretical background

The CLT approach for calculating the axial stiffness of the NCF composite specimen is very attractive due to its simplicity in application. The stiffness elements of a laminate with flat layers (NCF composite with zero waviness) are related to the A-matrix of the laminate

$$Q_{ij}^{LAM} = A_{ij}^{LAM}/h \qquad A_{ij}^{LAM} = \sum_{k=1}^{N} \bar{Q}_{ij}^{k}\, t_k \qquad \textbf{Eq. (1)}$$

For the NCF composite represented by laminate with effective layers we have

$$Q_{ij}^{NCF} = A_{ij}^{NCF}/h \qquad A_{ij}^{NCF} = \sum_{k=1}^{N} \bar{Q}_{ij}^{k-eff}\, t_k \qquad \textbf{Eq. (2)}$$

with $\overline{Q}_{ij}^{k-eff}$, t_k and h being the effective stiffness matrix of the layer in global coordinates, average layer thickness and average laminate thickness respectively. For the axial stiffness of a cross-ply laminate and the NCF composite analyzed in this paper we obtain

$$Q_{11}^{LAM} = Q_{11}^{0}\frac{t_0}{h} + Q_{22}^{90}\frac{t_{90}}{h} \qquad \textbf{Eq. (3)}$$

$$Q_{11}^{NCF} = Q_{11}^{0-eff}\frac{t_0}{h} + Q_{22}^{90-eff}\frac{t_{90}}{h} \qquad \textbf{Eq. (4)}$$

Q_{22}^{90-eff} is the effective transverse stiffness of the homogenized 90°-layer with varying thickness (t_{90} is the average thickness), Q_{11}^{0-eff} is the effective axial stiffness of the curved 0°-layer.

The stiffness knock-down factors for the 0°-layer, for the 90°-layer and for the NCF composite (represented by laminate) are introduced as follows

$$k_0 = \frac{Q_{11}^{0-eff}}{Q_{11}^{0}} \qquad k_{90} = \frac{Q_{22}^{90-eff}}{Q_{22}^{90}} \qquad k_{NCF} = \frac{Q_{11}^{NCF}}{Q_{11}^{LAM}} \qquad \textbf{Eq. (5)}$$

From **Eq. (5)** and **Eq. (4)** we obtain

$$Q_{11}^{LAM}k_{NCF} = k_0 Q_{11}^{0}\frac{t_0}{h} + k_{90}Q_{22}^{90}\frac{t_{90}}{h} \qquad \textbf{Eq. (6)}$$

Using **Eq. (3)** to replace Q_{11}^{0} , **Eq. (6)** can be rearranged in the form

$$k_{NCF} = k_0 + \Delta k \qquad \Delta k = (k_{90} - k_0)\frac{Q_{22}^{90} t_{90}}{Q_{11}^{LAM} h} \qquad \textbf{Eq. (7)}$$

The second term in **Eq. (7)** depends on the layer stiffness and thickness ratio and on the difference between the knock-down factors for the 0°- and 90°-layer. Results presented in **Section 5** show that this term can be neglected without introducing any noticeable error. Certainly, to find these knock-down factors, we have to start with proper definition and methodology for determination of the effective stiffness.

The axial stiffness Q_{11}^{NCF} of symmetric and balanced NCF composite can be obtained from the macroscopic in-plane stress-strain relationship

$$\sigma_x^{NCF} = Q_{11}^{NCF}\varepsilon_x + Q_{12}^{NCF}\varepsilon_y \qquad \textbf{Eq. (8)}$$

In **Eq. (8)** x-direction is the specimen axial (loading) direction, see **Figure 1**. The NCF composite axial stiffness element Q_{11}^{NCF} is obtained performing FE-analysis for plane strain case ($\varepsilon_y = 0$). In this loading case Q_{11}^{NCF} is obtained directly dividing the calculated axial average stress by the macroscopic strain applied. The average stress is axial force F_x divided by nominal (average) thickness of the laminate h. Hence

$$Q_{11}^{NCF} = \frac{F_x}{h\varepsilon_x} \qquad \textbf{Eq. (9)}$$

The effective in-plane axial stiffness of the curved 0°-layer is lower than the stiffness of a straight layer mainly because the fibers are not oriented in-plane. However, as shown in **[20]**, the curved layer in addition to end loading (applied displacement) is subjected to large normal and tangential tractions at the layer interface. In other words the loading to the curved layer is not uniaxial and as a consequence the force calculated at the right end of the layer (index R) is not equal to the force on the left end (index L) , $F_x^R(0°) \neq F_x^L(0°)$. This makes the determination of the effective stiffness uncertain, because different values are obtained using different cross-sections. The same applies to the 90°-layer with varying thickness $F_x^R(90°) \neq F_x^L(90°)$. The numbers $0°$ and $90°$ in parenthesis indicate the layer under consideration. Certainly, on both ends the total force is the same, for example

$$F_x^R(0°) + F_x^R(90°) = F_x \qquad \textbf{Eq. (10)}$$

Because of the described reason the effective layer "stiffness" calculated on the left and the right edge of the model differs

$$Q_{11}^{R}(0°) \neq Q_{11}^{L}(0°) \quad Q_{22}^{R}(90°) \neq Q_{22}^{L}(90°) \qquad \textbf{Eq. (11)}$$

$$Q_{11}^{R}(0°) = \frac{F_x^R(0°)}{\varepsilon_x t_0} \quad , Q_{11}^{L}(0°) = \frac{F_x^L(0°)}{\varepsilon_x t_0}$$

$$, Q_{22}^{R}(90°) = \frac{F_x^R(90°)}{\varepsilon_x (t_{90}+A)} , Q_{22}^{L}(90°) = \frac{F_x^L(90°)}{\varepsilon_x (t_{90}-A)} \qquad \textbf{Eq. (12)}$$

In fact none of these numbers is stiffness, because the loading to the layer is not uniaxial. For the purpose of employing the CLT, the effective layer stiffness Q_{11}^{0-eff} and Q_{22}^{90-eff} have to be defined in a way that using **Eq. (2)** gives exactly the same values for NCF composite as direct FE calculation.

In **[20]** it was demonstrated that the following definitions of effective stiffness give this result

$$Q_{11}^{0-eff} = \frac{Q_{11}^{R}(0°)+Q_{11}^{L}(0°)}{2} \qquad \textbf{Eq. (13)}$$

$$Q_{22}^{90-eff} = \frac{Q_{22}^{R}(90)\frac{t_{90}+A}{t_{90}}+Q_{22}^{L}(90)\frac{t_{90}-A}{t_{90}}}{2} \qquad \textbf{Eq. (14)}$$

These definitions together with **Eq. (5)** will be used in all calculations.

4. FE modeling

In this paper the 0/90 units shown in **Figure 1b and Figure 1c** are analyzed. The thickness of the 0^o-layer is equal to the average thickness of one 90^o-layer, $t_0 = t_{90}$ .The top surface of the 0^o-layer in **Figure 1b** is traction free and all node belonging to the top surface of the unit in **Figure 1c** are coupled. The finite element code ANSYS14.0 with PLANE42 elements in plane strain assumption was used. The coordinate system of each element in the 0^o-layer followed the sinusoidal shape of the layer. The area of each layer was meshed with quadratic elements with 200 divisions along the model length and 40 divisions along the thickness direction. Symmetry condition was applied along the left vertical boundary and a constant x-

displacement was applied along the right vertical boundary leading to average strain in x-direction equal to 1%. Symmetry condition was applied along the bottom boundary.

Forces for effective stiffness determination according to **Eq. (12)-(14)** were calculated by summing the reaction forces acting on the nodes along the corresponding edge of the layer. The reaction force on the node shared by both layers is replaced by half of the reaction force of the neighboring node, by analogy with the reaction force on the upper-right node in the free upper boundary which is also equal to half of the reaction force of its neighboring node.

5. Numerical analysis: Results and discussion

5.1. NCF stiffness knock-down factor

In order to investigate which term (k_0 or Δk) is affecting more the NCF knock down factor in **Eq. (7)**, calculations are performed for two different ratios of wavelength L and the layer thickness t_0 : $L/t_0=10$ and $L/t_0=15$ and for both CF/EP and GF/EP materials for the unit with surface 0^o-layer. Results are presented in **Figure 2**. Although the knock down factors in the case of CF/EP are decreasing more than for the case of GF/EP, both figures present similar behavior of the curves and the same conclusions can be deduced for both materials. The term Δk in **Eq. (7)** can be neglected since it is almost equal to zero in the figures. Thus, the NCF composite knock down factor defined by **Eq. (5)** can be assumed equal to the 0^o-layer knock down factor defined by **Eq. (5)** and **Eq. (13)**, $k_{NCF} \backsimeq k_0$. In other words, in order to know NCF cross-ply composite knock down factor, it is enough to know the 0^o-layer knock down factor.

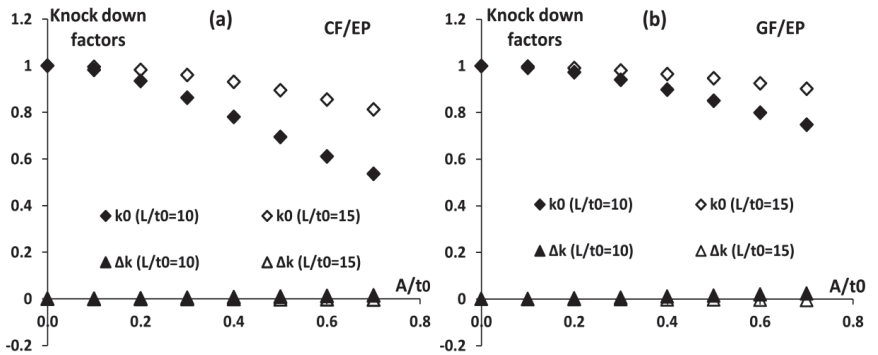

Figure2. Comparison of k_0 and Δk in the expression of NCF knock- down factor in **Eq. (7)** for unit with surface 0°-layer **(a)** CF/EP and **(b)** GF/EP

In the following, the focus will be mostly on the determination of knock down factor of the 0°-layer. An important observation deduced from **Figure 2** is that the curves of k_0 corresponding to $L/t_0=10$ and $L/t_0=15$ look similar and have similar shape. This leads to assumption that both curves may coincide by performing proper "deformation" of both axis (changing scales). As a consequence the curve corresponding to $L/t_0=15$ could be obtained as a part of the curve corresponding to $L/t_0=10$. More generally: Is it possible to predict the knock down factor for any L/t_0 ratio as a function of A/t_0 based on known relationship for one given L/t_0 ratio which could be considered as a master curve? As shown in the next section the answer is "yes". It is suggested to determine the master curve by performing accurate FE calculations for the case of short wavelength L/t_0 and to fit it with analytical function.

5.2. Master curve approach

5.2.1. Knock down-factor curve and fitting function

The case of $L/t_0=6$ is considered as extreme case where the same amplitude can lead to a steep angle of the waviness. The 0°-layer knock-down factor is decreasing more than in cases with larger ratios. The knock-down factor dependence on the wave amplitude at $L/t_0=6$ will be considered as master curve for the rest of calculations. The analytical fitting of the case of $L/t_0=6$ will be used to calculate the knock-down

factors for the other cases of the higher ratios of L/t_0. The calculated values and the fitting curves are presented in **figure 3** for both materials and for the unit with surface 0^o-layer. The same fitting expression in **Eq. (15)** is found for both materials.

$$k_0 = \frac{1}{1+b\,(A/t0)^c} \qquad \textbf{Eq. (15)}$$

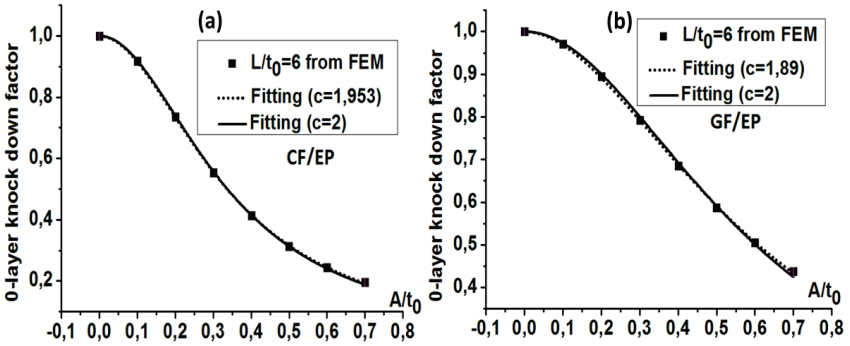

Figure3. Fitting function for Master curve (L/t_0 =6) (surface 0^o-layer) **(a)** CF/EP and **(b)** GF/EP

The fitting constants "b" and "c" are given in **Table 2** for both CF/EP and GF/EP materials and for both surface and embedded 0^o-layer cases.

Table2. Fitting constants

	Surface 0^o-layer		Embedded 0^o-layer	
	b	c	b	c
CF/EP	8.39	1.95	4.95	1.95
	8.78	2	5.14	2
GF/EP	2.56	1.89	1.51	1.86
	2.77	2	1.64	2

The fitting constant c is weakly dependent on the material system and in following it is considered as a material independent and set equal to 2. The new constant "b" is then found according to the new c (c=2) in order to get the best possible fitting. This means that only one parameter "b" depending on the material properties is remaining in the **Eq. (15)**. The **Eq. (15)** seems to be rather "universal" for all materials. Then, for instance, even one single FE calculation is enough to determine this parameter.

5.2.2. Validation and application of the master curve approach

In this section the aim is to demonstrate and identify the relationship between knock-down factor curves for different combinations of L/t_0 and A/t_0. Then we will explain how the master curve is used to predict the 0^o-layer knock down factor degradation for any case of L/t_0.

The procedure as it is illustrated in **Figure 4** is the following. We consider the knock-down factor curves for two different wavelength values L/t_0. . We assume that one of them is the master curve (in our selection it is the curve for $L/t_0=6$, denoted $\mathrm{k_{0M}}$ (Index M is for Master) and the other one corresponds to a different wavelength $L/t_0=n$, denoted $\mathrm{k_{0n}}$. We select an arbitrary value of the knock-down factor, $\mathrm{k_0^*}$ on both curves and denote the corresponding values of the amplitude $(\mathrm{A/t0})_{\mathrm{M}}^*$ and $(\mathrm{A/t0})_{\mathrm{n}}^*$.

$$k_{0M}((A/t0)_M^*) = k_0^* \qquad k_{0n}((A/t0)_n^*) = k_0^* \qquad \textbf{Eq. (16)}$$

Using data in **Figure 4** we can produce a new figure where on the horizontal axis we have

$$\mathrm{a} = \frac{(A/t0)_M^*}{(A/t0)_n^*} \cdot (A/t0)_n \qquad \textbf{Eq. (17)}$$

In **Eq. (17)** $(\mathrm{A/t0})_{\mathrm{n}}$ is the variable value of the amplitude for $\mathrm{k_{0n}}$ curve. In the new figure each knock-down factor curve is differently "deformed" in the horizontal direction according to the first term in **Eq. (17)**. In new coordinates $(\mathrm{a}, \mathrm{k_0})$ the two considered points $((\mathrm{A/t0})_{\mathrm{M}}^*, \mathrm{k_0^*})$ and $((\mathrm{A/t0})_{\mathrm{n}}^*, \mathrm{k_0^*})$ coincide (the $\mathrm{a}-$coordinate is the same). Generally speaking, there is no reason to expect that other points on these curves would coincide too. However, the results presented in **figure 5** for CF and GF for the case of unit with surface 0^o-layer show that the curves coincide. The extremely high degree of agreement of numerical results for all inspected materials and also embedded layers (**Figure 1c**) as well, indicates that there may be an exact correlation which we do not know at present. These results imply that knock down factor k_{0n} curves for all possible wavelength $L/t_0 = n$ values coincide when they are

plotted against $a = \frac{(A/t0)^*_M}{(A/t0)^*_n} . (A/t0)_n$. Applying **Eq. (17)** to the master curve we have $a = (A/t0)_M$. Hence, **Eq. (17)** can be written as

$$(A/t0)_M = \frac{(A/t0)^*_M}{(A/t0)^*_n} \cdot (A/t0)_n \qquad \textbf{Eq. (18)}$$

The numerically established relationship **Eq. (18)** between both curves allows for a simple recalculation routine: for any selected knock-down factor k_0 and $(A/t0)_M$ on the master curve we can find the value of amplitude $(A/t0)_n$ that would give the same knock-down factor for wavelength $L/t_0=n$

$$(A/t0)_n = \frac{(A/t0)^*_n}{(A/t0)^*_M} \cdot (A/t0)_M \qquad \textbf{Eq. (19)}$$

To use **Eq. (19)** we first have to find $(A/t0)^*_n$ and $(A/t0)^*_M$.

An illustration of the procedure is shown in the following figures for CF composite and for surface 0°-layer case. The knock-down factor curve for L/t_0 =6, shown in **Figure 3**, is a master curve represented by fitting expression **(15)**. It is used to find $k_{0n}(A/t_0)$ for n=10.

We perform FE calculation for n=10 waviness with one chosen value of the amplitude $(A/t0)^*_{10} = 0.7$. The calculated knock-down factor is $k^*_0 = 0.536$. From **Eq. (15)**

$$k^*_0 = \frac{1}{a+b\cdot\left((A/t0)^*_M\right)^c} \qquad \rightarrow \quad \boldsymbol{(A/t0)^*_M = 0.312}$$

Then a set of values of $(A/t0)_M$ is chosen (first row in **Table 3**). The corresponding values of k_0 (second row) are calculated from **Eq. (15)**. Finally **Eq. (19)** is used to calculate corresponding values of $(A/t0)_{10}$.

Table3. Calculation results (For CF/EP) (Unit with surface 0°-layer)

$\boldsymbol{(A/t0)_M}$	0	0.05	0.10	0.15	0.20	0.25	0.30	$\boldsymbol{(A/t0)^*_M}$**=0.312**
$\boldsymbol{k_0}$	1	0.98	0.91	0.83	0.73	0.64	0.56	**0.536**
$\boldsymbol{(A/t0)_{10}}$	0	0.11	0.22	0.34	0.45	0.56	0.67	0.70

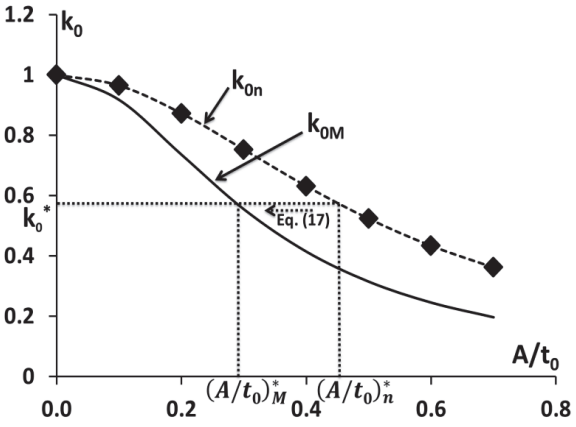

Figure4. Master curve approach

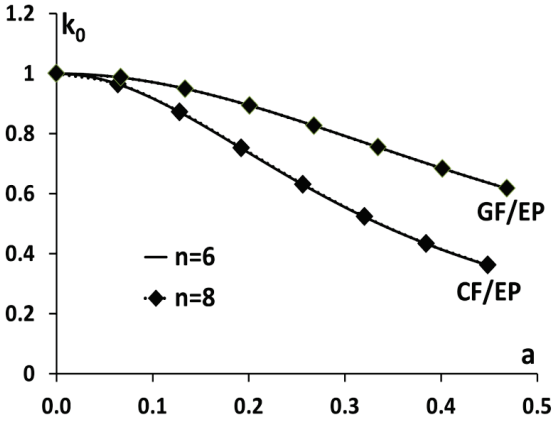

Figure5. Figure 4 after calculation using **Eq. (17)** for the case of *LM/t₀=6* and *Ln/t₀=8*, for CF/EP and GF/EP and for the unit with surface 0°-layer.

The 0°-layer knock down factors k_0 given in the second row in **Table 3** are plotted as a function of $(A/t0)_{10}$ given in the third row of the same table. Thus the 0°-layer knock down factor curve is obtained for the case of *L/t₀=10* using the fitting expression of the master curve and only one FE calculation for amplitude *A/t₀=0.7* for *L/t₀=10*. The results presented in **Figure 6a** are for CF/EP material as well as for GF/EP. The fitting constant c in **Eq. (15)** is assumed equal to 2 for both materials. The obtained knock-down curve is plotted at the same figure with knock down facture

curve calculated using FE for the same case of $L/t_0=10$. The master curve approach is thereby shown to give a good agreement within the considered range of amplitude and wavelength.

The same procedure is applied for $L/t_0=15$ composite (see **Figure 6b**). And the same is done for the unit with embedded 0^o-layer as well (see **Figure 7a** and **Figure 7b**).

The assumption of making c=2 is working well for both units and the only remaining unknown constant is "b" in the fitting expression. Which means few FE calculated data points can be enough to determine the unknown constant "b" in the equation of the master curve and another FE-calculation data point to predict the whole behavior of the knock down factor at a different wavelength.

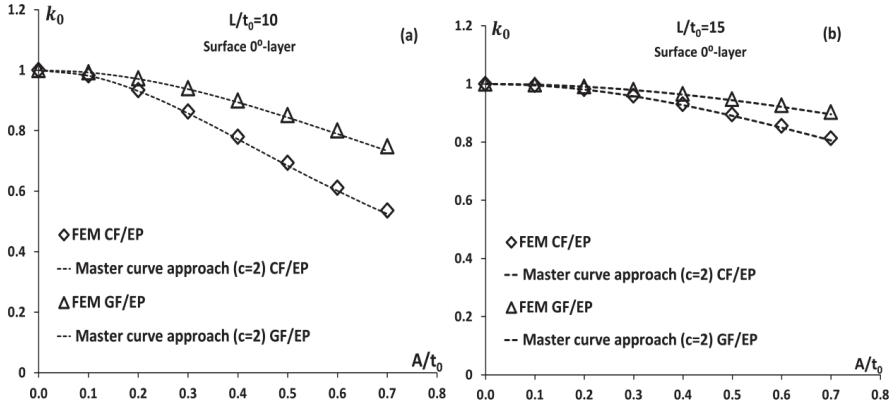

Figure6. Comparison of k_0 calculated using FE with k_0 calculated using master curve approach for unit with surface 0^o-layer **(a)** $L/t_0=10$ and **(b)** $L/t_0=15$.

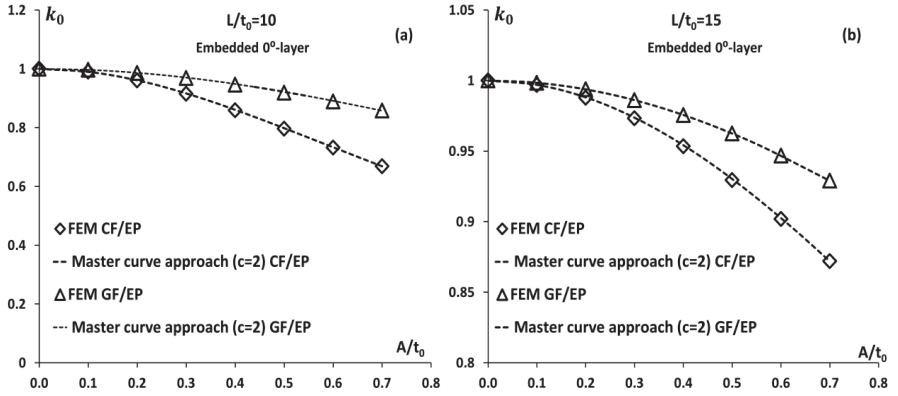

Figure7. Comparison of k_0 calculated using FE with k_0 calculated using master curve approach for unit with embedded 0^o-layer **(a)** *L/t$_0$=10* and **(b)** *L/t$_0$=15*.

Finally k_{NCF} is calculated in **Eq. (7)** using k_0 determined from the master curve approach together with k_{90} calculated from **Eq. (5)** and **Eq. (14)**. The results are presented in **Figures 8-9** and are compared to direct FE calculation for NCF knock down factor. If k_{90} is used equal to 1 means that the effective stiffness of the 90^o-layer is considered equal to the transverse stiffness of the UD composite material, and the effect of the waviness and thickness variation on the 90^o-layer effective stiffness is neglected. The results corresponding to this case in **Figures 8-9** are close to the results using **Eq. (7)** and k_{90} calculated using **Eq. (5)** and **Eq. (14)**. On the other hand, k_0 determined using master curve approach is rather close to the NCF knock down factors calculated directly from FE. . Since $\mathrm{k_0 < k_{NCF}}$, it can be used as a conservative estimation of the NCF composite axial stiffness reduction.

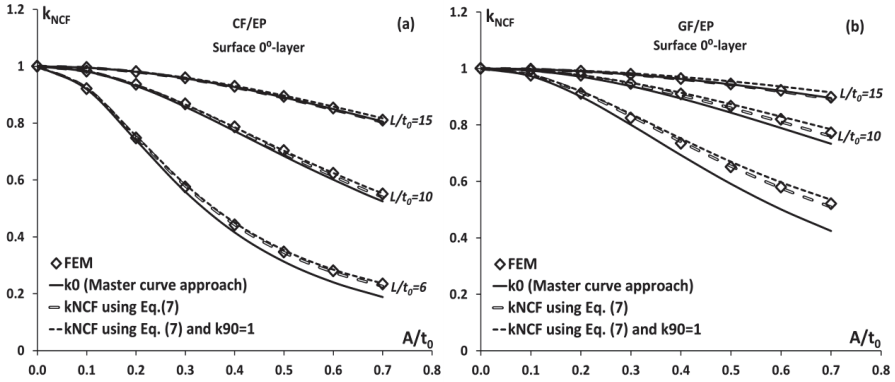

Figure8. NCF composite knock down factor with surface 0^{o}-layer **(a)** CF/EP **(b)** GF/EP.

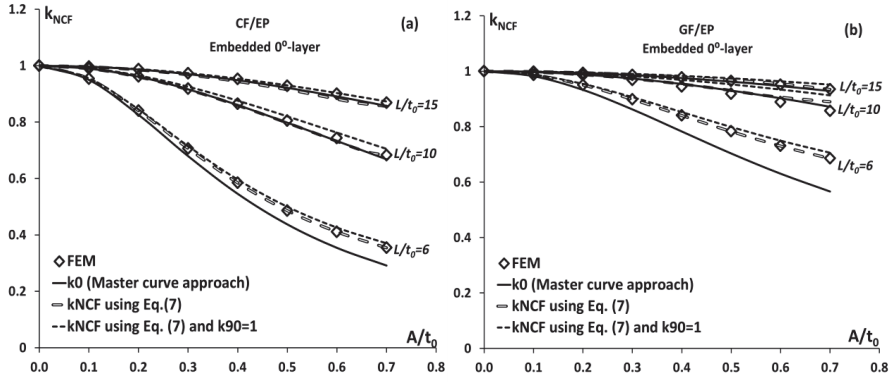

Figure9. NCF composite knock down factor with embedded 0^{o}-layer **(a)** CF/EP **(b)** GF/EP.

Conclusions

Numerical parametric FE-analysis showed that the axial stiffness reduction (knock-down factor) of a cross-ply type NCF composite made of carbon fiber (CF) or glass fiber (GF) bundles with out-of-plane waviness of a surface 0-^{o}layer or embedded 0-^{o}layer is almost the same as the effective stiffness reduction of the curved 0^{o}-layer. This conclusion holds for a large variety of wavelength and wave amplitudes of imperfections.

Analyzing the calculated 0^o-layer knock-down factor versus the wave amplitude curves for NCF composites with different wavelength we observed that these curves for different wavelength can be reduced to one master curve by changing the scale of the wave amplitude axis.

It was found analyzing results for CF and GF cases that the numerical data building the master curve can be fitted by a very simple one-parameter function. Thus, for a given material only a few FE calculations for a selected wavelength and amplitude is all what is needed to construct the master curve. More calculations would serve the validation purpose.

To construct the 0^o-layer knock-down factor versus wave amplitude curve for a different wavelength only one FE calculation is required for arbitrary selected amplitude. Predictions performed for CF and GF NCF composites show a very good agreement with direct FE calculations. Without losing accuracy, transverse stiffness of the 90-layer material can be used to represent the effective transverse stiffness of the 90-layer. The knock-down factor of the 0-layer is as a lower bond of the NCF composite stiffness reduction.

The observed features used in the master curve approach require further investigation regarding their mechanical origin and potential of application to more complex NCF composites with 0^o-layer waviness.

Acknowledgements

It is gratefully acknowledged that the work performed in this paper is partly funded by the Swedish 5th National Aeronautical Research Program (NFFP5) through the project ReFACT, and also through the Joint European Doctoral Program in Material Science and Engineering (DocMase).

References

[1] Dransfield K, Baillie C, Yiu-Wing M. Improving the delamination resistance of CFRP by stitching – a review. Composites Science and Technology 1994; 50: 305-317.

[2] Dransfield K, Jain L, Mai, Y-W. On the effects of stitching in CFRPs- I. Mode I delamination toughness. Composites Science and Technology 1998; 58: 815-827.

[3] Jain L, dransfield K, Mai, Y-W. On the effects of stitching in CFRPs- II. Mode II delamination toughness. Composites Science and Technology 1998; 5: 829-837.

[4] Leong KH, Ramakrishna S, Huang ZM, Bibo GA. The potential of knitting for engineering composites- a review. Composites: Part A 2000; 31: 197-220.

[5] Drapier S, Wisnom MR. Finite-element investigation of the compressive strength of non-crimp-fabric based composites. Composite Science and Technology 1999;59:1287-1297.

[6] Drapier S, Wisnom MR. A finite-element investigation of the interlaminar shear behaviour of non-crimp-fabric-based composites. Composite Science and Technology 1999;59:2351-2362.

[7] Miller AJ. The effect of microstructural parameters on the mechanical properties of non-crimp fabric composites. M. Phil. thesis, Cranfield University, School of Industrial and Manufacturing Science 1996.

[8] Ishikawa T, Chou TW. Elastic behaviour of woven hybrid composites. Journal of Composite materials 1982; 16: 2-19.

[9] Ishikawa T, Chou TW. One-dimensional micromechanical analysis of woven fabric composites. AIAA Journal 1983; 21(12):1714-1721.

[10] Kurath P, Karayaka M. Deformation and failure behaviour of woven Composite Laminates. Journal of Engineering Materials and Technology 1994; 116: 222-232.

[11] Wang Y, Li J, Do PB. Properties of composites laminates reinforced with E-glass multiaxial non-crimp fabrics. Journal of Composite Materials 1995; 29(17): 2317-2333.

[12] Bibo GA, Hogg PJ, Kemp M. Mechanical characterisation of glass- and carbon-fibre-reinforced composites made with non-crimp fabrics. Composite Science and technology 1997; 57(9-10): 1221-1241.

[12] Chun H-J, Ryu KS, Byun JH. Predictions of Elastic Properties of Multi-axial Warp Knitted Fabric Composites. Key Engineering Materials 2004; 261-263(II): 1499-1504.

[13] Robitaille F, Clayton BR, Long AC, Souter BJ, Rudd CD.Geometric modelling of industrial preforms: warp-knitted textiles. Proceedings of the Institution of

Mechanical Engineers Part L, Journal of Materials: Design and Applications 2000; 214: 71-90.

[14] Klopp K, Veihelmann B, Kolkmann A, Laourine E, Gries. Use of reinforcement textiles in fiber reinforced plastics. Tech Text 2003; 46: 59-63.

[15] Tessitore N, Riccio A. A novel FEM model for biaxial non-crimp fabric composite materials under tension. Computers and Structures 2006; 84: 1200-1207

[16] Byström J., Jekabsons N, Varna J. An evaluation of different models for prediction of elastic properties of woven composites. Composites: Part B 2000; 31: 7-20.

[17] Mattsson HD, Varna J. Average strain in fiber bundles and its effect on NCF composite stiffness. Journal of Engineering materials and technology 2007; 129: 211-219.

[18] Edgren F, Asp LE. Approximate analytical constitutive model for non-crimp fabric composites. Composites: Part A 2005; 36: 173-181.

[19] Zrida H, Marklund E, Varna J, Ayadi Z. Effective stiffness of 0^o-layer for stiffness determination of cross-ply non-crimp fabric composites. Journal of reinforced plastics and composites 2014 (submitted)

[20] Marklund E, Asp LE, Varna J. Modelling stiffness and strength of non-crimp fabric composites semi-laminar analysis. Woodhead publishing in materials,Non-crimp fabric composites: manufacturing, properties and application 2011; 17:403-438.